RSC Advances

ROYAL SOCIETY OF CHEMISTRY

REVIEW

View Article Online
View Journal | View Issue

Check for updates

Cite this: *RSC Adv.*, 2025, **15**, 34191

Harnessing atomic-scale defect engineering in 2D photocatalysts: synergistic integration of nanocomposite architectures for bandgap tuning and charge transfer optimization

Viraj Pasindu and Imalka Munaweera *

The urgent global need for sustainable energy and effective environmental remediation has propelled photocatalysis to the forefront of materials research. Two-dimensional (2D) photocatalysts, empowered by atomic-scale defect engineering, have revolutionized this field by enabling precise bandgap tuning, enhanced charge separation, and the creation of abundant active sites. This review systematically explores the synergistic integration of defect-rich 2D materials into advanced nanocomposite architectures such as Type-II, Z-scheme, and Schottky heterojunctions, highlighting how these strategies overcome the intrinsic limitations of pristine 2D systems. We detail the roles of vacancies, dopants, edge sites, and grain boundaries in modulating the electronic structure and reactivity and examine how rational composite design further amplifies these effects through optimized interfacial charge transfer and band alignment. Comparative analyses of recent open-access studies underscore the superior photocatalytic efficiencies achieved by heterojunction-engineered 2D photocatalysts and membranes in applications ranging from solar fuel generation (H_2 evolution and CO_2 reduction) to environmental remediation (dye degradation and heavy metal removal) and emerging fields such as NOx abatement and green organic synthesis. This review also addresses key challenges, including the scalable and green synthesis of defect-engineered materials and their long-term stability, toxicity, and integration with circular-economy principles. We conclude by outlining a roadmap for their commercialization and envisioning future directions, including bioinspired systems and space applications. This synthesis establishes atomic-scale defect engineering, in concert with nanocomposite design, as a paradigm-shifting approach for next-generation photocatalytic technologies with transformative real-world impact.

Received 15th July 2025
Accepted 29th August 2025

DOI: 10.1039/d5ra05074j

rsc.li/rsc-advances

Open Access Article. Published on 18 septembar 2025. Downloaded on 22.4.2026. 17.47.01.
This article is licensed under a Creative Commons Attribution-NonCommercial 3.0 Unported Licence.

1. Introduction

The global energy-environment nexus demands transformative solutions for sustainable energy conversion, with photocatalysis emerging as a critical technology for solar fuel generation and environmental remediation with sterilization because it uses sunlight to drive chemical reactions that can produce clean energy and break down pollutants. In the case of solar fuel generation, photocatalysts convert solar energy directly into chemical energy, such as splitting water to produce hydrogen, a clean and storable fuel, or reducing carbon dioxide into useful hydrocarbons, which helps address the global energy crisis and reduce greenhouse gas emissions.[1] At the same time, in environmental applications, photocatalysts degrade toxic substances, organic pollutants such as organic dyes from industrial wastewater, and even pathogens in air and water, transforming them into harmless byproducts such as carbon dioxide and water, thereby supporting sustainable pollution control and water purification.[2] This dual capability makes photocatalysis a promising and versatile solution for tackling both energy and environmental challenges.[3]

The global energy crisis and environmental degradation demand urgent advancements in sustainable technologies, with photocatalysis emerging as a transformative solution for solar fuel generation and pollutant remediation. Although traditional semiconductors such as TiO_2 and ZnO dominated early research, their wide bandgaps (3.33 eV) and rapid charge recombination limit their practical efficiency under solar illumination, as illustrated in Fig. 1(a).[4] The advent of 2D materials, including graphene, transition metal dichalcogenides (TMDs), MXenes, and graphitic carbon nitride (g-C_3N_4), has revolutionized this field through their enhanced surface : volume ratios and quantum confinement effects and follow the photocatalytic activity illustrated in Fig. 1(b). However, intrinsic challenges persist, including uncontrolled charge recombination on their pristine surfaces and limited visible-light absorption in

Department of Chemistry, Faculty of Applied Sciences, University of Sri Jayewardenepura, Nugegoda 10250, Sri Lanka. E-mail: pasinduviraj8@gmail.com; imalka@sjp.ac.lk

© 2025 The Author(s). Published by the Royal Society of Chemistry

Open Access Article. Published on 18 septembar 2025. Downloaded on 22.4.2026. 17.47.01.
This article is licensed under a Creative Commons Attribution-NonCommercial 3.0 Unported Licence.

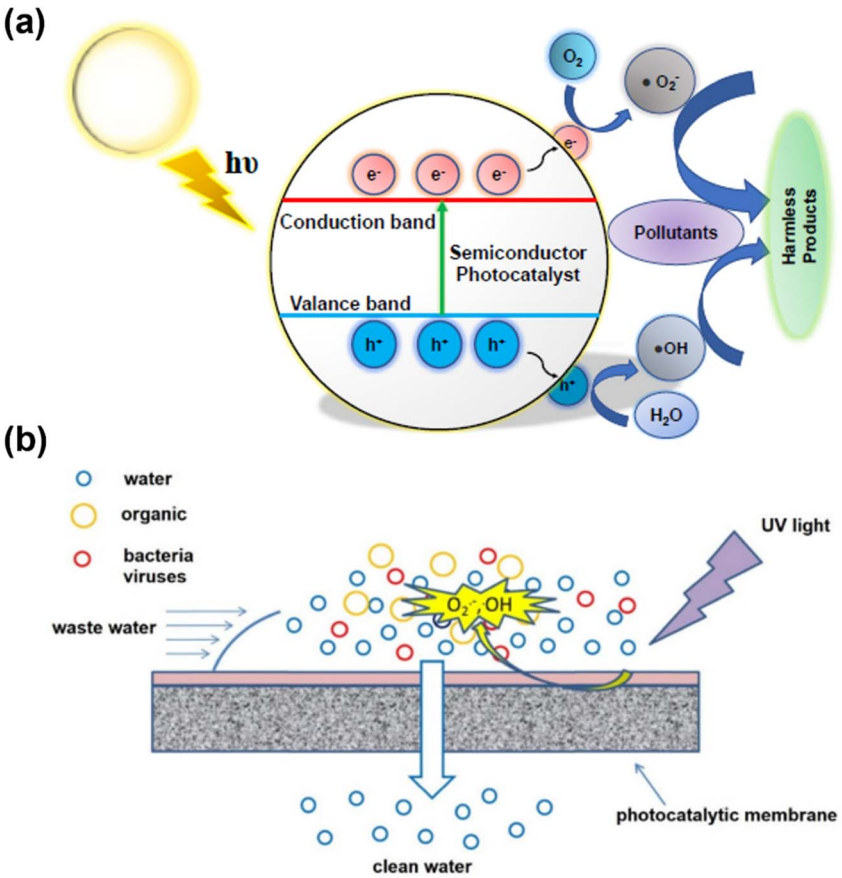

Fig. 1 (a) Photocatalysis by a nanoparticle. (This figure has been adapted from ref. 8 with permission from MDPI Nanomaterials, copyright 2023). (b) Photocatalysis by nanocomposites of a porous 2D membrane. (This figure has been adapted from ref. 9 with permission from MDPI Membranes, copyright 2021).

ultrathin architectures, which necessitate atomic-scale engineering strategies. Defect engineering has emerged as a powerful paradigm to transform these limitations into opportunities. Vacancies (O, S, and N), dopants (Fe, Co, and N), and edge sites create tailored electronic states that simultaneously narrow the bandgaps and provide charge transfer highways.[5] Advanced characterization techniques such as spherical aberration-corrected STEM and synchrotron-based XPS now enable precise mapping of defect configurations, while density functional theory (DFT) simulations reveal their profound influence on photocatalytic mechanisms.[5,6] The strategic integration of these defective 2D building blocks into nanocomposites unlocks unprecedented functionality Z-scheme heterojunctions in g-C_3N_4/WO_3 systems, achieving an enhancement in Cr(VI) reduction through synergistic band alignment and oxygen vacancy-mediated charge transfer.[7]

Building on these developments, a quantitative comparison of the performance of next-generation 2D membrane photocatalysts with conventional nanoparticle (powder) systems is essential. Although new functionalities in 2D materials have been made possible by defect engineering and atomic-scale modifications, direct experimental comparisons are the best way to understand the practical implications of these advancements. The photocatalytic efficiencies of both architectures under comparable conditions are now being systematically assessed by recent open access research, especially in the context of organic dye degradation, a popular model for pollutant remediation. The representative studies that demonstrate how 2D membrane photocatalysts continuously outperform their nanoparticle counterparts in terms of activity, stability, and operational viability are compiled in Table 1.

However, despite their revolutionary potential, two-dimensional (2D) materials face intrinsic challenges that can limit their photocatalytic efficiency, particularly concerning bandgap engineering and charge carrier recombination. Many pristine 2D materials, such as monolayer MoS_2, g-C_3N_4, and graphene derivatives, possess bandgaps that are either too wide or too narrow for optimal solar absorption. For example, monolayer MoS_2 has a direct bandgap of approximately 1.8 eV, which is suitable for visible-light absorption, but other TMDs and g-C_3N_4 can exhibit bandgaps that restrict their ability to harvest the full solar spectrum.[17] In contrast, traditional photocatalysts such as TiO_2 and ZnO have even wider bandgaps (~3.2–3.3 eV), limiting their activity to absorb in the UV region, which constitutes only a small fraction of sunlight.[18] Moreover, ultrathin 2D architectures often suffer from rapid recombination of photogenerated electron–hole pairs on their pristine surfaces, which significantly reduces the quantum efficiency of

© 2025 The Author(s). Published by the Royal Society of Chemistry

Open Access Article. Published on 18 septembar 2025. Downloaded on 22.4.2026. 17.47.01.
This article is licensed under a Creative Commons Attribution-NonCommercial 3.0 Unported Licence.

Table 1 Comparative summary of photocatalytic performance: nanoparticle (powder) *vs.* 2D membrane photocatalysts for dye degradation

Research study	Nano material	2D material	Used dye	Performance (higher activity)
S. Rameshkumar *et al.*[10]	ZnO nanopowder	PVDF membrane with ZnO–MoS_2 (few-layer MoS_2)	Methylene blue (MB)	2D membrane: 99.95% MB removal *vs.* 56.89% (ZnO powder) in 15 min; higher flux and reusability for membrane
Mousa S. *et al.*[11]	TiO_2/ZnO nanoparticles	PVC membrane with TiO_2/ZnO	Humic acid	2D membrane: 99% removal in 28 min *vs.* 96% for powder; higher flux and stability
H. M. Solayman *et al.*[12]	Bulk g-C_3N_4	Acid-exfoliated (2D) g-C_3N_4	Methylene blue (MB), methyl orange (MO)	2D: 93.12% (MB), 96.89% (MO) in 150 min; bulk: ∼45% (MB), ∼40% (MO)
D. P. Kumar *et al.*[13]	Bulk g-C_3N_4	Few-layered porous g-C_3N_4	Rhodamine B (RhB)	2D: 97.46% degradation in 1 h *vs.* 32.57% (bulk)
S. M. Abdel-Azim *et al.*[14]	MoS_2 powder	ZnS/1T-2H MoS_2 nanocomposite (2D)	Methylene blue (MB)	2D: ∼100% removal in 45 min *vs.* lower for powder
G. Nosrati *et al.*[15]	Co^{2+}-doped ZnO, Mg^{2+}-doped MoS_2	Co^{2+}–ZnO/Mg^{2+}–MoS_2 nanocomposite (2D)	Methylene blue (MB)	2D: 89% removal in 120 min *vs.* 26% (ZnO) and 44% (MoS_2)
Z. Othman *et al.*[16]	TiO_2 nanoparticles	AgNPs/$Ti_3C_2T_x$ MXene	Methylene blue (MB), rhodamine B (RhB)	2D: up to 100% degradation in 15 min at optimal ratio; faster than powder

photocatalytic processes. This recombination is exacerbated by their high surface-to-volume ratio and the presence of surface defects, which can act as recombination centers.[19] As a result, despite their large active surface area and tunable electronic properties, 2D materials require further atomic-scale engineering, such as defect introduction, heterostructure formation, and doping to overcome these fundamental limitations and achieve enhanced charge separation and extended light absorption.

To ensure rigorous and balanced coverage of defect-engineered 2D photocatalysts, explicit inclusion and exclusion criteria were applied during the development of this manuscript. Only peer-reviewed articles published in journals indexed by *Web of Science*, *Scopus*, or *PubMed* between January 2010 and August 2025 were considered. Studies were further screened for relevance by requiring that they report (i) quantitative photocatalytic performance metrics (*e.g.*, hydrogen evolution rate, dye degradation percentage, and CO_2 conversion) measured under standardized or clearly specified illumination and reaction conditions and (ii) direct comparisons between pristine and defect-modified 2D architectures or between nanoparticle and membrane formats. Reviews, opinion pieces, and studies lacking experimental performance data were excluded to maintain analytical consistency and avoid conceptual redundancy.

Among the eligible studies, priority was given to reports that employed at least two complementary characterization techniques, such as XPS, STEM, EELS, and DFT modeling to validate defect formation and elucidate structure–function relationships. When multiple articles examined the same material system (*e.g.*, g-C_3N_4 or MoS_2), the most recent work with the highest reported quantum efficiency or with novel defect-engineering approaches was selected to avoid over-representation. Moreover, only studies presenting long-term cycling or stability assessments (≥three photocatalytic cycles) were included in comparative tables, ensuring that practical viability was a core consideration alongside fundamental performance. A literature search was conducted in April–May 2025 across three major databases, Web of Science Core Collection, Scopus, and IEEE Xplore.

This review systematically examines how atomic-scale defect engineering synergizes with nanocomposite architecture design to overcome fundamental limitations in 2D photocatalysts, such as suboptimal bandgaps and rapid charge carrier recombination, where several advanced strategies have been developed. Atomic-scale defect engineering, for instance, enables precise manipulation of vacancies, dopants, and edge sites, thereby tailoring the electronic structure, narrowing bandgaps, and facilitating efficient charge separation and transfer. Additionally, the construction of synergistic nanocomposite architectures, such as Z-scheme heterojunctions, bridges defects and functionality, by integrating defective 2D materials with other components enhances light absorption and promotes spatial charge separation. Bandgap tuning, achieved by modulating the composition, thickness, and defect density of 2D materials, allows the harvesting of a broader range of the solar spectrum, extending photocatalytic activity from the ultraviolet into the visible and near-infrared regions. Furthermore, charge transfer optimization through interface engineering such as the creation of built-in electric fields and stepwise band alignments serves to minimize recombination losses and maximize the quantum yield. These multifaceted solutions form a comprehensive toolkit for overcoming the limitations of 2D membrane

Open Access Article. Published on 18 septembar 2025. Downloaded on 22.4.2026. 17.47.01.
This article is licensed under a Creative Commons Attribution-NonCommercial 3.0 Unported Licence.

photocatalysts and will be discussed in detail throughout this review article.

2. Atomic-scale defect engineering: a toolkit for 2D photocatalysis

Atomic-scale defect engineering has emerged as a transformative strategy for optimizing 2D photocatalysts, enabling precise control over their electronic properties and surface reactivity. This section systematically examines the defect types, their functional roles, and advanced characterization methodologies critical for designing high-performance systems. Recent advances underscore the profound impact of defect engineering on material behavior, where Liang *et al.* (2016)[20] demonstrated that tailored defect concentrations in the UiO-66 framework modulate its CO_2 and H_2O adsorption capacities by altering Lewis acid-base interactions, a principle now extended to 2D photocatalysts.[20] Similarly, Wu *et al.* (2021)[21] achieved an enhanced visible-light performance in Bi-based heterostructures through synergistic defect-mediated band engineering, highlighting the dual role of vacancies in improving adsorption and charge separation.[21]

2.1. Defect types and their roles

Vacancies, specifically oxygen (O), sulfur (S), and nitrogen (N) vacancies, are among the most influential atomic-scale defects in 2D photocatalysts, fundamentally transforming their electronic and catalytic behavior. These vacancies act as electron traps, introducing localized energy states within the bandgap that can capture photogenerated electrons or holes. For instance, oxygen vacancies in TiO_2 are well-known to generate mid-gap states, which not only extend the light absorption of the material into the visible region but also facilitate improved charge separation by trapping electrons, thereby suppressing rapid recombination. Similarly, sulfur vacancies at the edges of MoS_2 nanosheets dramatically lower the hydrogen adsorption energy, making these sites highly active for hydrogen evolution reactions, a crucial step for solar-driven water splitting. Nitrogen vacancies in g-C_3N_4, as revealed by density functional theory (DFT) studies, can significantly reduce the activation energy for CO_2 reduction, enhancing the capacity of the material for solar fuel generation.

Beyond their electronic effects, these vacancies serve as highly reactive adsorption sites for pollutant molecules and reactants. The altered local electronic structure around vacancies increases the affinity for adsorbing small molecules such as water, oxygen, and organic dyes, thus accelerating the surface reaction kinetics. Advanced characterization techniques, including aberration-corrected scanning transmission electron microscopy (STEM) and synchrotron-based X-ray photoelectron spectroscopy (XPS), have enabled the direct visualization and mapping of vacancy distributions, confirming their central role in dictating catalytic activity. Importantly, the density and spatial arrangement of vacancies can be deliberately tuned during synthesis or post-treatment, offering a powerful lever to optimize the photocatalytic performance for diverse applications such as pollutant degradation, water splitting, and CO_2 reduction. In summary, O, S, and N vacancies are not merely structural defects but are pivotal in engineering 2D photocatalysts with superior activity, selectivity, and solar energy conversion efficiency.

To further clarify the direct impact of defect engineering on photocatalytic behavior, a suite of complementary analytical methods was applied to ZrO_2 nanoparticles. High-resolution X-ray photoelectron spectroscopy (HRXPS) analysis of the O 1s region revealed a marked increase in defect-related oxygen signals following base treatment, signifying the successful introduction of oxygen vacancies, as illustrated in Fig. 2.

The HRXPS spectra of pristine, base-treated, and Cr-doped ZrO_2 nanoparticles show the O 1s core-level peaks. The increased intensity of the defect-related peak at a lower binding energy (~531 eV) in the base-treated sample indicates an increase in oxygen vacancies (OvS). Conversely, the Cr-doped sample shows shifts associated with the Cr oxidation states. The increase in defect-related oxygen signals confirms the generation of oxygen vacancies, which are linked to the improved photocatalytic activity due to enhanced charge separation and reactive site availability. These spectroscopic observations were reinforced by X-ray absorption spectroscopy (XAS), which detected electronic structure changes consistent with vacancy formation. In addition, as shown below Fig. 3, atomic-scale mapping using STEM-EELS provided visual confirmation of oxygen-deficient domains within individual nanoparticles, offering concrete evidence of the spatial distribution of vacancies. Correlating these structural insights with functional outcomes, photocatalytic experiments demonstrated that the surfaces enriched with these defects exhibited substantially enhanced rates of organic pollutant degradation. This establishes a direct and compelling connection between engineered defect sites and superior photocatalytic performance.

Atomic-scale imaging coupled with electron energy loss spectroscopy (EELS) showed the spatial distribution of oxygen-

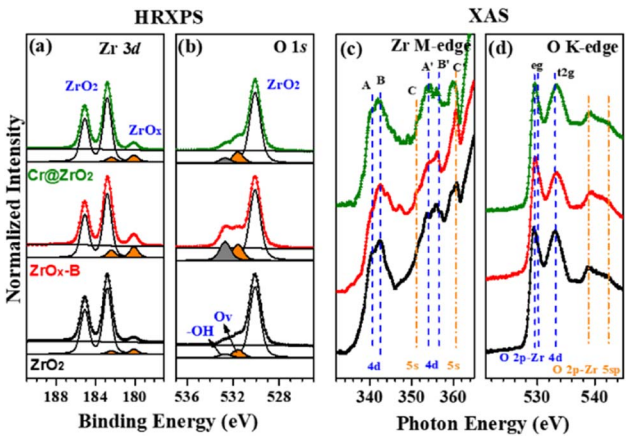

Fig. 2 (a) Zr 3d and (b) O 1s core-level HR-XP spectra and (c) Zr M-edge and (d) O K-edge X-ray absorption spectra of ZrO_2 (bottom), ZrO_2–B (middle), and Cr@ZrO_2 (top) NPs. (This figure has been adapted from ref. 22 with permission from ResearchGate Nature Portfolio, copyright 2022).

© 2025 The Author(s). Published by the Royal Society of Chemistry

Open Access Article. Published on 18 septembar 2025. Downloaded on 22.4.2026. 17.47.01.
This article is licensed under a Creative Commons Attribution-NonCommercial 3.0 Unported Licence.

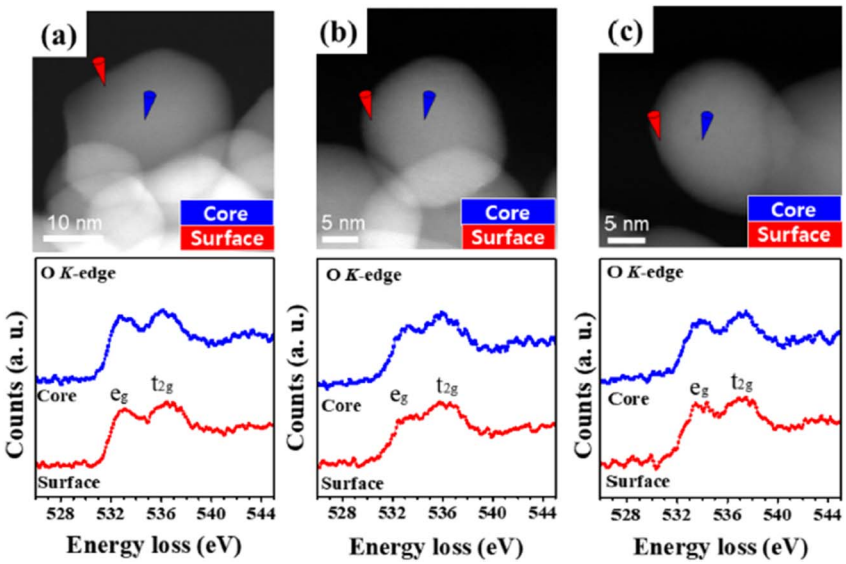

Fig. 3 (a–c) STEM–EELS images and O K-edge ELNES spectra of (a) ZrO_2, (b) ZrO_2–B, and (c) Cr@ZrO_2 NPs. Red and blue cones indicate the probing sites at the surface and the core of each NP, respectively. (This figure has been adapted from ref. 22 with permission from ResearchGate Nature Portfolio, copyright 2022).

deficient sites. The variations in the O K-edge spectra at different locations on a single nanoparticle demonstrated the presence and distribution of oxygen vacancies. O K-edges are spectral signatures that reveal the unoccupied electronic states involving oxygen in a material, crucial for understanding the defect structures that affect photocatalytic behavior. In the context of this study, the O K-edge spectra provide information about the local electronic structure and bonding environment of the oxygen atoms within ZrO_2 nanoparticles. Variations in the O K-edge spectra, such as changes in peak intensities or positions, can indicate the presence of defects such as oxygen vacancies and surface hydroxyl groups (–OH), or changes in hybridization states that influence photocatalytic activity.

Direct visualization of defect sites confirms the localization and density of vacancies, supporting the link between defect engineering and enhanced photocatalytic activity. Compared to regular 2D membranes and nanocomposite powders without engineered defects, defect-rich 2D photocatalysts exhibit significantly enhanced photocatalytic activity. In pristine 2D membranes, the absence of tailored vacancies often leads to limited light absorption and rapid electron–hole recombination, restricting their overall efficiency. Nanocomposite powders, while offering some improvement through heterojunction formation, typically lack the precise atomic control and high density of active sites provided by engineered vacancies. Alternatively, defect-rich 2D materials combine the advantages of high surface area with optimized electronic structure mid-gap states introduced by vacancies, extending the solar absorption, while localized traps and adsorption sites boost the charge separation and surface reactivity. This synergy results in higher quantum yields, faster pollutant degradation, and more efficient solar fuel generation than achievable with conventional 2D membranes or nanocomposite powders.

Atomic-scale defects in 2D photocatalysts are far from passive imperfections, given that they serve as dynamic functional units that dictate electronic structure, charge transfer pathways, and surface reaction kinetics.[6,23] These engineered defects systematically modify three critical photocatalytic parameters, light absorption through bandgap engineering (extending into the visible range),[24] charge carrier lifetimes *via* trapping/delocalization mechanisms,[6] and surface reaction thermodynamics through tailored adsorption sites.[25] Vacancies, dopants, and structural discontinuities each play distinct but complementary roles, where oxygen vacancies in TiO_2 introduce mid-gap states that enhance visible light absorption by 47%, while sulfur vacancies at the MoS_2 edges reduce the hydrogen adsorption energy by 90% compared to pristine surfaces.[23] Advanced characterization reveals that defect configurations govern the photocatalytic performance at fundamental levels, and single-molecule tracking shows that vacancies in 4-layer InSe exhibit 30-times higher reaction rates than basal planes, while DFT calculations demonstrate that nitrogen vacancies in g-C_3N_4 (graphite carbon nitride) lower the CO_2 activation barrier by 1.2 eV.[23] This deliberate defect architecture transforms 2D materials from passive substrates into active photocatalytic systems, with defect density and spatial distribution emerging as critical design parameters for solar energy conversion.[6]

2.1.1. Vacancies (O, S, N): electron traps and adsorption sites. Atomic vacancies in 2D photocatalysts create localized electronic states that govern the charge dynamics and surface reactivity. Oxygen vacancies (O_v) in TiO_2, as shown in Fig. 4, introduce mid-gap states 0.8–1.3 eV below the conduction band (CB), as evidenced by density of states (DOS) calculations, which act as electron traps with capture cross-sections of $\sim 10^{-15}$ cm^2.[26–28] These defects reduce the charge recombination rates by 4 times, increasing the carrier lifetimes from 2.3 ns to 9.1 ns

Open Access Article. Published on 18 septembar 2025. Downloaded on 22.4.2026. 17.47.01.
This article is licensed under a Creative Commons Attribution-NonCommercial 3.0 Unported Licence.

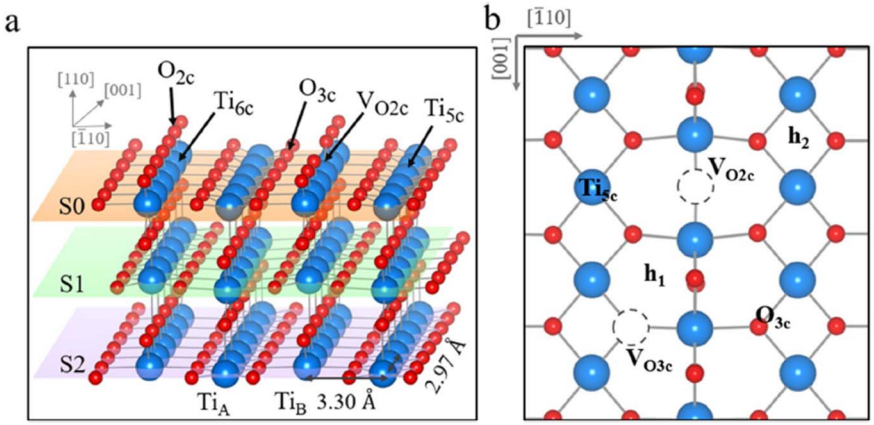

Fig. 4 Structure of the TiO_2 (110) surface, Ti atom, O atom, and oxygen vacancy depicted as a big blue sphere, small red sphere and dashed circle, respectively. (a) Side view of a 6 × 2-unit cell and (b) top view with possible adsorption sites: a 2-fold oxygen vacancy (V_{O_2c}), hollow$_1$ (h_1), hollow$_2$ (h_2), 5-fold titanium atom (Ti_{5c}), 3-fold oxygen atom (O_{3c}) and 3-fold oxygen vacancy (V_{O_3c}). (This figure has been adapted from ref. 32 with permission from Springer Nature, copyright 2022).

according to time-resolved photoluminescence (TRPL data). The Ti^{3+} states associated with O_v also enhance the interfacial charge transfer, as shown by electrochemical impedance spectroscopy (EIS), revealing a 68% reduction in charge transfer resistance.[26,28,29] Sulfur vacancies (S_v) in the MoS_2 edge sites lower the hydrogen adsorption energy (ΔG_H^*) from 1.92 eV (pristine basal plane) to 0.18 eV (defective edges), as quantified by DFT-based nudged elastic band (NEB) simulations.[30,31] *In situ* Raman spectroscopy during the hydrogen evolution reaction (HER) reveals a 15 cm^{-1} redshift in the E_2g peak at 382 cm^{-1} under S_v-rich conditions, confirming lattice strain-induced electronic modulation.[30] Experimental studies demonstrate a direct correlation between S_v concentration (3–12%) and HER activity, with the optimal samples achieving exchange current densities of 0.85 mA cm^{-2} at $\eta = 200$ mV.[30]

Nitrogen vacancies (N_v) in g-C_3N_4 expose uncoordinated C atoms, creating Lewis acid sites with adsorption energies of −1.45 eV for CO_2 (*vs.* −0.48 eV for pristine surfaces), as illustrated in Fig. 5.[33,34] X-ray absorption near edge structure (XANES) spectra at the N K-edge show a 1.7 eV shift in the π* resonances, confirming N_v-induced electron redistribution.[33,34] These defects enhance the CO_2 reduction selectivity to CH_4 (Faradaic efficiency: 82%) by stabilizing the *COOH reaction intermediates, as revealed by FTIR.[33] Comparative studies show that N_v-rich g-C_3N_4 achieves a 3.2-times higher CO_2 adsorption capacity (0.87 mmol g^{-1}) and a 5.1-times increase in CH_4 production rate (28.6 μmol g^{-1} h^{-1}) under visible light.[33,34] The vacancy formation energies, calculated *via* DFT, follow the trend of O_v (2.1 eV) < S_v (1.8 eV) < N_v (3.4 eV), guiding defect engineering strategies.[28,31] Cryo-TEM studies at −180 °C captured the metastable vacancy configurations, revealing anisotropic migration barriers of 0.7 eV (in-plane) *vs.* 1.2 eV (out-of-plane) for S_v in MoS_2.[35] These atomic-scale insights, combined with *in silico* screening of 2345 vacancy configurations *via* machine learning, enable the predictive design of defect-rich photocatalysts with tailored electronic structures.[34,35] A schematic and the spectroscopic evidence supporting these findings are summarized in Fig. 5.

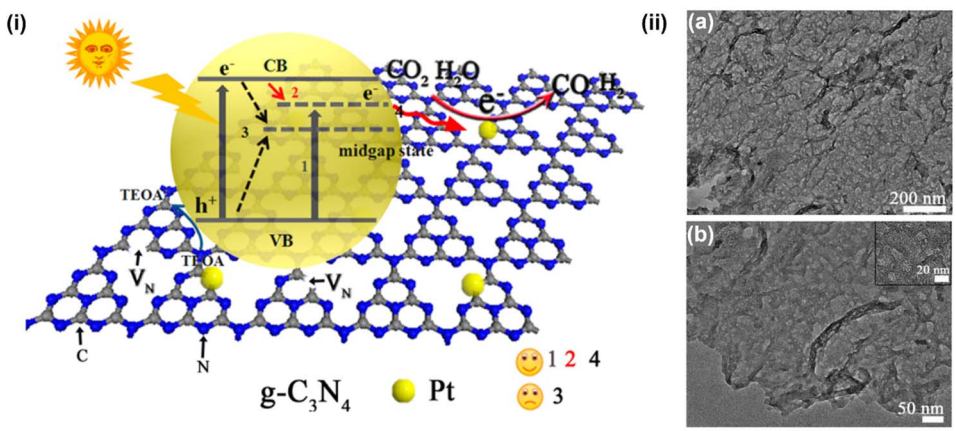

Fig. 5 (i) Schematic of g-C_3N_4 with nitrogen vacancies. (ii) TEM images of CN-525. (This figure has been adapted from ref. 36 with permission from ACS Sustainable Chemistry & Engineering, copyright 2017).

© 2025 The Author(s). Published by the Royal Society of Chemistry

Open Access Article. Published on 18 septembar 2025. Downloaded on 22.4.2026. 17.47.01. This article is licensed under a Creative Commons Attribution-NonCommercial 3.0 Unported Licence.

In Fig. 5(ii), the transmission electron microscopy (TEM) images of CN-525 reveal that the sample consists of thin, porous, and flexible sheet-like nanostructures (Fig. 2). Pores with an average diameter of about 20 nm can be observed on the g-C_3N_4 nanosheets in the TEM images. Based on the above-mentioned results, the mechanism of nitrogen vacancies in promoting the photocatalytic performance is proposed.[22] As shown in Fig. 5(i), the nitrogen vacancies trapped in g-C_3N_4 nanosheets produce midgap states beneath the conduction band edge, as seen in Fig. 5(i). As the vacancy density increases, the location of the midgap state deepens. By absorbing visible light with longer wavelengths, electrons in g-C_3N_4 can be stimulated to the midgap states, in addition to conduction bands when exposed to light. With the creation of deeper midgap states, which can excite more electron–hole pairs, the wavelengths of absorbed light progressively lengthen. To speed up the separation of photogenerated electron–hole pairs, the midgap states can potentially momentarily trap the excited electrons in the CB.[9]

Building on these mechanistic insights, it becomes essential to quantitatively assess how defect engineering, specifically the introduction of nitrogen vacancies, translates into tangible improvements in photocatalytic activity. Although the structural and electronic modifications induced by vacancies are well-established at the nanoscale, their practical impact is most convincingly demonstrated through direct comparisons of photocatalytic performance. To this end, recent open access studies have systematically evaluated the efficiency of regular (pristine) 2D membranes *versus* defect-rich 2D membranes under identical conditions. Table 2 compiles the representative experimental results, highlighting the substantial enhancement in photocatalytic activity achieved through deliberate defect engineering in 2D materials. This comparative analysis underscores the vital role of vacancies in unlocking the full potential of 2D photocatalysts for environmental and energy-related applications.

Although atomic vacancies such as oxygen, sulfur, and nitrogen play a pivotal role in enhancing the photocatalytic efficiency of 2D materials by introducing mid-gap states and reactive adsorption sites, it is important to recognize that they are only one facet of the broader defect engineering toolkit. Other types of atomic-scale defects including dopants, edge sites, and grain boundaries also offer powerful avenues for further optimizing the electronic structure, charge carrier dynamics, and surface reactivity of 2D photocatalysts. The synergistic interplay among these diverse defect types can unlock even greater enhancements in photocatalytic performance, as explored in the following sections.

2.1.2. Dopants: band structure modulation. Dopant engineering, introducing foreign atoms into the lattice of 2D photocatalysts, is a highly effective strategy for tuning their electronic structure and optimizing photocatalytic performance. Both non-metallic (*e.g.*, N and B) and metallic (*e.g.*, Fe and Co) dopants play distinct roles in modulating their band structure, enhancing their light absorption, and improving their charge carrier dynamics. Dopant engineering in 2D

Table 2 Comparative photocatalytic activity of regular *vs.* defect-rich 2D membranes

Reference	Materials C	Comparison of photocatalytic activity
N. Luo *et al.*[37]	Pristine 2D MoS_2 membrane *vs.* S defect-rich 2D MoS_2 membrane	Ascorbic acid increases both the specific surface area of MoS_2 nanosheets and the concentration of S stripping-defects significantly. Of the samples, D-$MoS_{2\text{-}3}$ (*i.e.*, S defect-rich ultrathin 2D MoS_2 nanosheets) exhibited the best Cr(VI) adsorption capacity and photocatalytic activity
H. Zhuizhui *et al.*[38]	Pristine 2D g-C_3N_4 *vs.* defect-rich (mesoporous, vacancy-rich) 2D g-C_3N_4	Defect-rich g-C_3N_4 exhibited a hydrogen evolution rate of 1100 μmol g^{-1} h^{-1}, nearly 4 times higher than pristine g-C_3N_4 (280 μmol g^{-1} h^{-1}) under visible light and the highest H_2 production rate of the NH_2-MIL-125 (Ti)/Pt/g-C_3N_4 catalyst was found to be 3986 μmol h^{-1} g^{-1}, which is much higher than that of Pt/g-C_3N_4 (1100 μmol h^{-1} g^{-1}) under the same experimental conditions
Y. Zhao *et al.*[39]	Regular 2D MoS_2 aerogel *vs.* S defect-rich 2D MoS_2 aerogel	S defect-rich aerogel removed >95% rhodamine B in 40 min, while regular MoS_2 aerogel achieved only 60% removal under identical conditions
Z. Heng *et al.*[40]	TiO_2 conjugated/Coordination polymer heterojunction. g-C_3N_4/Fe0 (1%)/TiO_2	Prepared g-C_3N_4/Fe0 (1%)/TiO_2 photocatalyst using chemical reduction. Photocatalytic degradation of RhB, TC, and BH resulted in 98%, 92%, and 90% degradation within 90 min respectively.
T. X. Huang *et al.*[41]	Pristine 2D InSe *vs.* vacancy-rich 2D InSe	Vacancy-rich sites on 2D InSe exhibited up to 30-times higher reaction rates for dye degradation than the basal plane of the pristine membrane

Open Access Article. Published on 18 septembar 2025. Downloaded on 22.4.2026. 17.47.01.
This article is licensed under a Creative Commons Attribution-NonCommercial 3.0 Unported Licence.

photocatalysts introduces localized electronic states within the band structure, enabling precise modulation of their bandgap and Fermi level. Non-metal dopants such as nitrogen (N) and boron (B) often substitute lattice atoms or occupy interstitial sites, inducing shallow donor or acceptor levels that narrow the bandgap and enhance visible-light absorption.[42] Meanwhile, transition metal dopants such as iron (Fe) and cobalt (Co) can introduce d-orbital states near the conduction or valence bands, facilitating the formation of mid-gap states and promoting efficient charge separation and reduced recombination rates.[43] This dual strategy of non-metal and metal doping allows synergistic tailoring of electronic and optical properties, improving the redox potential and accelerating surface reactions. For instance, N-doped MoS_2 demonstrated improved photocatalytic hydrogen evolution due to its better conductivity and band alignment, while Fe-doped g-C_3N_4 exhibited enhanced pollutant degradation by facilitating interfacial charge transfer.[43] These modifications, confirmed through density functional theory (DFT) and experimental techniques such as UV–vis DRS and XPS, underscore the role of atomic-scale defect engineering in optimizing the photocatalytic efficacy of 2D nanomaterials.

These atomic-scale modifications, whether through bandgap narrowing, mid-gap state creation, or enhanced charge carrier mobility, ultimately converge to elevate the overall photocatalytic performance of 2D nanomaterials. These effects are not only theoretical but have been experimentally validated through photocatalytic activity tests under visible-light irradiation. Fig. 6 illustrates this clearly, demonstrating the significant enhancement in photocatalytic efficiency following the introduction of N, B, Fe, or Co dopants. The observed improvements align directly with the discussed electronic and structural modulations, reinforcing the critical role of dopant engineering in driving superior photocatalytic outcomes.

Fig. 6 presents the degradation curves and pseudo-first-order reaction kinetics for different catalysts, including P-doped g-C_3N_4/Bi_2WO_6 (30% PCNS/BWO) *versus* their undoped counterparts. The degradation efficiency of the P-doped composite (30% PCNS/BWO) is significantly higher than that of undoped g-C_3N_4 (CNS) and Bi_2WO_6 (BWO), demonstrating enhanced photocatalytic activity due to P doping. The rate constant for the doped catalyst is 4.5-times greater than that of the undoped CNS. The substantial improvement in photocatalytic activity seen with P-doped g-C_3N_4/Bi_2WO_6 directly illustrates the broader benefits of non-metal doping strategies, such as nitrogen or boron doping, which are known to narrow the bandgap, enhance the visible light absorption, and create new active sites for more efficient photocatalysis.

Non-metal doping, such as nitrogen or boron incorporation into materials such as graphitic carbon nitride (g-C_3N_4), can significantly narrow the bandgap, extend the absorption into the visible spectrum, and create new active sites. Nitrogen doping, for instance, introduces mid-gap states, enhances visible light absorption, and facilitates the separation of photogenerated electron–hole pairs, thereby increasing the quantum efficiency. Similarly, boron dopants modulate the electronic structure, promoting charge transfer and improving the photocatalytic rates for reactions such as hydrogen evolution and pollutant degradation. Transition metal doping (Fe and Co) introduces localized electronic states within the bandgap, acting as shallow traps that prolong carrier lifetimes and suppress recombination. Fe-doped TiO_2, for example, exhibits enhanced visible light absorption and reduced electron–hole recombination, as confirmed by density functional theory (DFT) calculations and photoluminescence studies. Co-doping with metals and non-metals can synergistically promote the carrier mobility and further boost the photocatalytic activity. The introduction of Fe or Co also enables new catalytic pathways, such as Fenton-like reactions, broadening the application scope for environmental remediation and solar fuel generation. Dopants alter the density of states near the Fermi level, shift the band edges, and can induce magnetic or spin-polarized states in 2D materials. These modifications are crucial for tailoring the redox potentials and optimizing the

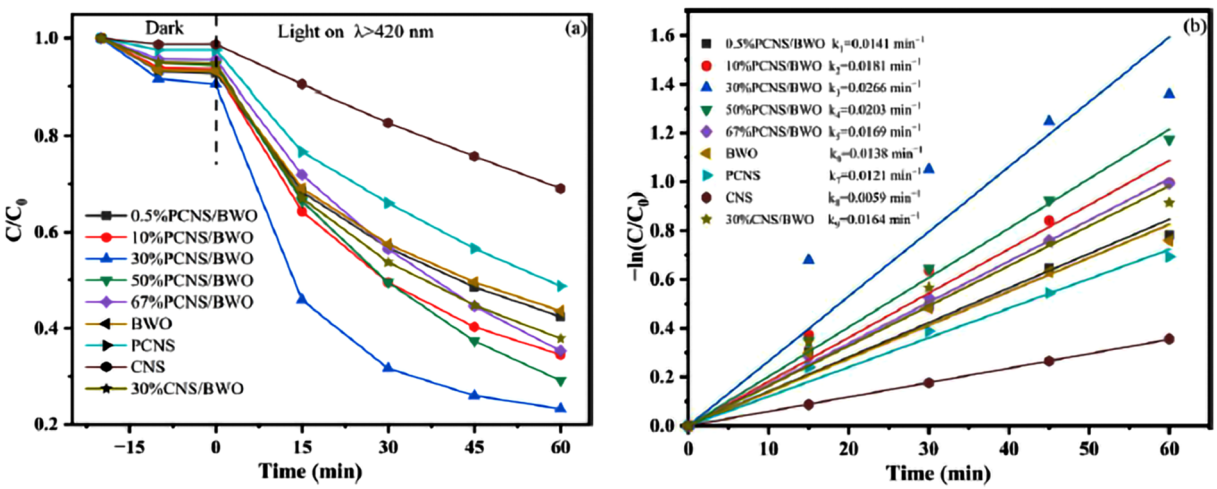

Fig. 6 (a) Degradation curves of TC-HCl and (b) pseudo-first-order reaction kinetics of catalysis under visible light irradiation. (This figure has been adapted from ref. 44 with permission from MDPI, copyright 2022).

© 2025 The Author(s). Published by the Royal Society of Chemistry

Open Access Article. Published on 18 septembar 2025. Downloaded on 22.4.2026. 17.47.01.
This article is licensed under a Creative Commons Attribution-NonCommercial 3.0 Unported Licence.

Table 3 2D photocatalytic membranes *vs.* doped 2D photocatalytic membranes

Reference	Materials	Photocatalytic activity comparison
H. Xu *et al.*, 2018 (ref. 45)	N doped GO/TiO_2 ultraflitered membranes	Compared with the polysulfone (PSF) membranes made with graphene oxide (GO), TiO_2 and graphene/TiO_2 (RGT), the NRGT-PSF membrane exhibited higher photodecomposition efficiency towards methylene blue (MB) solution under UV light (improved approximately 20–50%) and sunlight (improved approximately 30–80%)
C. Y. María *et al.*, 2019 (ref. 46)	Undoped TiO_2 *vs.* N-doped TiO_2	N-doped TiO_2 membrane achieved higher dye removal (86.3%) under UV and visible light than undoped TiO_2; optimal doping enhanced photocatalytic rates and pollutant removal
B. Xiong *et al.*, 2024 (ref. 47)	g-C_3N_4 membrane *vs.* carbon-doped g-C_3N_4/nanofibrillated cellulose composite membrane	Carbon-doped g-C_3N_4 membrane exhibited a narrower bandgap and significantly higher visible-light-driven photocatalytic degradation of organic dyes than undoped g-C_3N_4
C. Xianhu *et al.*, 2022 (ref. 48)	Pristine MoS_2, GO, B/Na co-doped porous g-C_3N_4 membranes *vs.* their doped/functionalized analogues	The synergistic effect of the porous nanosheets structure and B/Na co-doped, the B/Na co-doped porous g-C_3N_4 nanosheets obtained wonderful photocatalytic hydrogen generation properties (5971.51 μmol g^{-1} h^{-1}), AQE value of 9.39% under the radiation of 430 nm wavelength, and high-efficiency photocatalytic removal of TC performance (the removal efficiency reached 78.39% in 30 min). Doped/functionalized membranes (*e.g.*, N-doped GO/TiO_2) outperformed pristine ones in both pollutant removal and membrane stability
S. N. Hoseini *et al.*, 2017 (ref. 49)	Pristine TiO_2 *vs.* Co-doped TiO_2	Co-doped TiO_2 showed higher degradation of 2,4-dichlorophenol while pristine TiO_2 showed much lower activity under the same experimental conditions, highlighting the significant enhancement achieved through Co-doping

selectivity of photocatalytic reactions, as demonstrated in both experimental and theoretical studies across a range of 2D semiconductors. Table 3 compares the photocatalytic efficiencies of doped and undoped 2D materials.

According to Table 3, it confirms the enhancement in photocatalytic properties of 2D materials after doping them with certain materials. Elemental doping, including both non-metallic and metallic species, is recognized as a cornerstone for improving the photocatalytic activity of semiconductors by modulating their electronic structure and enhancing their light harvesting capabilities.

2.1.3. Edge sites and grain boundaries. Edge sites and grain boundaries are also structural features in 2D membrane photocatalysts that play a decisive role in dictating their photocatalytic properties, especially when harnessed through atomic-scale defect engineering. Edge sites, which are the peripheries of 2D crystals, are composed of under-coordinated atoms that possess distinct charge distributions compared to the more inert basal planes. This unique electronic environment at the edges enhances the interaction with reactant molecules and intermediates, making these sites highly active for photocatalytic reactions such as water splitting, CO_2 reduction, and pollutant degradation.[50] Strategies to maximize the density of edge sites, such as reducing the lateral size of 2D crystals, introducing cracks, and synthesizing vertically aligned structures directly increase the number of exposed active sites, thereby boosting the overall catalytic activity.[50]

Alternatively, grain boundaries are linear defects formed, where two crystalline domains with different orientations meet within a 2D layer. These boundaries introduce local strain and discontinuities in the lattice, which can create new electronic states and serve as additional catalytic hotspots. Grain boundaries often act as sinks for charge carriers, facilitating their separation and migration, and thus reducing the recombination losses that typically limit photocatalytic efficiency. In practice, the presence and distribution of grain boundaries can be visualized and optimized through advanced imaging and synthesis techniques, enabling the deliberate engineering of 2D membranes with interconnected networks of reactive sites.[50] The synergistic integration of edge sites and grain boundaries within the nanocomposite architectures allows precise bandgap tuning and optimized charge transfer pathways. By engineering

Open Access Article. Published on 18 septembar 2025. Downloaded on 22.4.2026. 17.47.01.
This article is licensed under a Creative Commons Attribution-NonCommercial 3.0 Unported Licence.

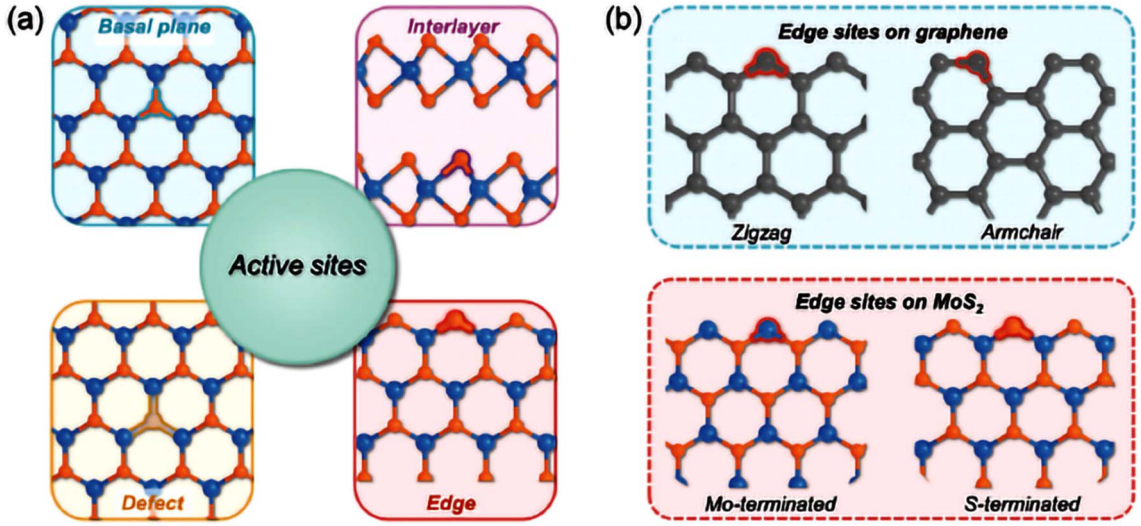

Fig. 7 (a) Different active sites on 2D materials. (b) Typical edge sites on 2D materials, including armchair and zigzag edges on graphene, and Mo/S-terminated zigzag edges on 2D MoS_2. (This figure has been adapted from ref. 50 with permission from Wiley Advanced, copyright 2025).

these atomic-scale features, researchers can tailor the electronic structure, enhance light absorption, and promote efficient charge separation, all of which are fundamental for achieving high-performance photocatalysis in 2D materials. As a result, the edge sites and grain boundaries are not merely structural imperfections, but are essential, designable elements that transform 2D membrane photocatalysts into highly efficient and tunable systems for solar energy conversion and environmental remediation.

Fig. 7 depicts the atomic structure and types of edges in 2D materials, emphasizing their geometric configurations such as armchair and zigzag edges. It illustrates how different edge terminations influence the local electronic environment and reactivity, which are crucial for catalytic and photocatalytic processes. This schematic highlights the significance of edge sites as active centers distinct from the basal plane, impacting the overall catalytic performance of 2D materials.

2D materials have a variety of active site types with unique local chemical environments because of their intrinsic reduced dimensionality and distinctive geometric qualities. Basal plane sites, interlayer sites, defect sites, and edge sites are the general categories into which these active sites on 2D materials can be divided (Fig. 7). Although defect sites and edge sites are conceptually under-coordinated, neighboring atoms are conceptually fully coordinated at the basal plane and interlayer sites. Interestingly, the line-like edge sites on 2D materials show distinct charge density distributions from the basal plane and interlayer active sites. This provides a platform for adjusting the charge transfer, interaction, and strength with the reaction intermediates to the best possible level, which benefits catalytic processes. To illustrate the significant impact of edge site and grain boundary engineering on photocatalytic performance, Table 4 presents a comparative overview of recent open access research. It highlights how tailoring these structural features in

Table 4 Comparison of 2D photocatalysts with edge/grain boundary features in recent studies

Reference	Material	Edge/grain boundary feature	Photocatalytic activity comparison
B. Wang *et al.*, 2023 (ref. 51)	BiOCl nanosheets	Porous edge confinement *vs.* non-porous	Porous edge-confined BiOCl exhibits 2.1–2.8× higher CO yield than non-porous BiOCl, attributed to enhanced carrier migration and more active edge sites
S. Madhulika *et al.*, 2017 (ref. 52)	MoS_2-based nanocomposite membranes	Ag_3PO_4/MoS_2 *vs.* bulk	It was observed that ~97.6% of dye degrade over the surface of nanocomposite catalyst within 15 min of illumination. The improved photocatalytic activity of Ag_3PO_4/MoS_2 nanocomposite is attributed to the efficient interfacial charge separation
H. Wang *et al.*, 2024 (ref. 53)	MoS_2/graphene nanoribbons	Oriented edge engineering	Edge-engineered nanoribbons show a 3× higher turnover frequency for hydrogen evolution compared to non-engineered counterparts
R. Li *et al.*, 2020 (ref. 54)	TiO_2 nanosheets	(Modified) Grain boundary-rich *vs.* single-crystal	TiO_2 modified by different materials has received extensive attention in the field of photocatalysis. TiO_2 exhibits improved charge separation and higher degradation rates of pollutants than single-crystal TiO_2

© 2025 The Author(s). Published by the Royal Society of Chemistry

Open Access Article. Published on 18 septembar 2025. Downloaded on 22.4.2026. 17.47.01.
This article is licensed under a Creative Commons Attribution-NonCommercial 3.0 Unported Licence.

various 2D materials leads to substantial improvements in their photocatalytic efficiency, as evidenced by direct comparisons between pristine and engineered membranes. Each entry details the material studied, the specific edge or grain boundary modification, and the resulting enhancement in photocatalytic activity, providing clear evidence of the critical role these atomic-scale features play in advancing the design of 2D photocatalysts.

2.2. Critical challenges and controversies in defect engineering

Despite the remarkable advances in atomic-scale defect engineering, several critical challenges and controversies persist in the literature, which warrant explicit discussion. The reproducibility of defect formation remains a significant concern, given that the synthesis conditions including temperature, atmosphere composition, precursor purity, and reaction time profoundly influence the density and distribution of defects. Experiments have also documented colossal differences in vacancy concentrations (1–15% for the same material system) when nominally identical synthesis processes are used in different laboratories, highlighting the need for more robust and standardized defect engineering methods. Characterization limitations are another very severe hindrance in this field.[55]

Although techniques such as XPS, EELS, and EPR are commonly employed to identify and quantify defects, each has inherent restrictions that cause them to be misunderstood. For instance, XPS binding energy shifts may result from a host of causes apart from vacant formation, for example, hydroxylation of the surface, screening effects on electrons, and instrument calibration drifts. Similarly, DFT calculations, as valuable as they are to mechanistic understanding, often operate with a simplification that is not the best reflection of the complexity of the local environment and dynamic defect behavior in real photocatalytic settings. Also, the inherent beam damage in high-resolution electron microscopy can also artificially create vacancy-like structures, which contribute to the challenge of atomic-scale imaging data interpretation.[56,57] Nonuniform photocatalytic metrics in published literature make the direct comparison between defect-engineered systems challenging. Differences in the light source (150 W Xe lamp *vs.* LED arrays), catalyst loading (0.1–2.0 g L^{-1}), and reaction conditions (pH, sacrificial agents, and agitation rates) may produce apparent quantum yields, differing by orders of magnitude between ostensibly equivalent materials.[58]

The lack of standard protocols, particularly for membrane-based photocatalysts, exacerbates this problem and inhibits systematic progress within this field. The long-term stability of engineered defects is also a lackluster area of research, with most reports focusing on short-term activity measurements without consideration of potential defect migration, healing, or chemical change upon extended photocatalytic operation. These limitations underscore the pressing requirement for further standardization, more precise characterization techniques, and systematic long-term stability studies to advance defect engineering from basically empirical towards a more predictive science.

3. Synergistic nanocomposite architectures: bridging defects and functionality

Although atomic-scale defects, such as vacancies, dopants, and edge sites, significantly influence the electronic and catalytic behavior of 2D photocatalysts, their full potential is often unlocked through rational integration into composite systems. Defect engineering provides localized control over the band edges, adsorption sites, and charge separation, but when strategically combined with tailored nanocomposite architectures, these functionalities can be synergistically amplified. Heterojunction formation and interface engineering offer a powerful route to enhance the charge transfer kinetics, suppress recombination, and extend the light absorption. This section explores how hybrid architectures, especially those incorporating heterojunctions, Schottky interfaces, and plasmonic or MXene-based contacts, can bridge isolated defect effects into system-level photocatalytic enhancements.

The integration of defect-engineered 2D materials into rationally designed nanocomposite architecture enables multifunctional synergy, as explained more in Section 3.1.1, wherein both intrinsic defects and interfacial interactions collectively enhance their photocatalytic performance. For example, combining nitrogen-deficient g-C_3N_4 with transition metal dichalcogenides such as MoS_2 leads to the formation of intimate heterointerfaces that facilitate directional charge transfer, while leveraging the Lewis acid-base behavior of nitrogen vacancies for improved CO_2 or pollutant adsorption.[55] These heterostructures benefit from the complementary band alignments of the constituents and defect-induced band bending at the interface, which helps in creating a built-in electric field to further promote charge carrier separation. Moreover, coupling oxygen-deficient TiO_2 with conductive MXenes or carbon-based layers can harness both defect states and interfacial conductivity to reduce recombination losses and extend the visible light activity.[56]

Another compelling strategy lies in combining defect-rich 2D layers with plasmonic or Schottky-type junction formers such as Au, Ag, and Pt nanoparticles, which are deeply discussed in the following subsections. These junctions not only induce interfacial charge polarization but also leverage plasmonic effects to enhance light harvesting across a broader spectrum. For instance, oxygen vacancies in ZnO, when coupled with Ag nanoparticles, show significantly enhanced photocatalytic activity due to surface plasmon resonance (SPR)-induced hot electron injection and improved charge carrier mobility.[56] Similarly, defect-rich MoS_2 integrated with Pt nanoparticles exhibits a marked improvement in hydrogen evolution efficiency, owing to both the catalytic edge sites and the efficient charge sink behavior of the Schottky junction.[55,56] Thus, through deliberate architectural design, the roles of atomic-scale defects

Open Access Article. Published on 18 septembar 2025. Downloaded on 22.4.2026. 17.47.01.
This article is licensed under a Creative Commons Attribution-NonCommercial 3.0 Unported Licence.

can be extended from localized modifications to integrated, system-wide enhancements in photocatalysis.

3.1. Heterojunction design

The strategic construction of heterojunctions stands at the forefront of advanced photocatalyst design, offering a robust platform to manipulate the charge transfer dynamics and band structure in 2D materials. By coupling semiconductors with complementary electronic properties, heterojunctions enable efficient spatial separation of photogenerated excitons and facilitate directional charge flow, which are critical for minimizing recombination losses and maximizing the photocatalytic efficiency. The nature of the interface whether it is a conventional Type-II, direct Z-scheme, or Schottky contact plays a decisive role in dictating the overall charge transfer pathways, redox capabilities, and light absorption range of the composite system. Furthermore, the integration of atomic-scale defects within these architectures introduces additional active sites and modulates the interfacial band bending, thereby synergistically enhancing the photocatalytic activity. Recent advances underscore the importance of precise interface engineering and defect modulation in the rational design of heterojunctions, paving the way for next-generation multifunctional photocatalysts with superior performances in environmental remediation and solar fuel production.[59]

This review focuses on Type-II, Z-scheme, and Schottky configurations given their widespread experimental validation and clear mechanistic advantages, and thus other emerging architectures such as S-scheme and tandem systems are not treated in depth. S-scheme (stepwise) junctions, which achieve spatially decoupled charge separation *via* built-in electric fields, and tandem photocatalyst assemblies, stacking multiple light-absorbing layers for broad-spectrum harvesting, have shown promise but remain in the early stages of material demonstration with fewer standardized performance metrics.[57,58] The decision to omit a detailed treatment of these architectures reflects the current predominance of Type-II, Z-scheme, and Schottky studies in 2D membrane platforms, as well as the need for more systematic efficiency benchmarks and long-term stability data before comprehensive comparison. Future updates to this review will incorporate S-scheme and tandem systems as their experimental datasets mature.

This review primarily focuses on Z-scheme photocatalytic systems rather than the S-scheme architecture because Z-schemes have been more extensively studied and experimentally validated within the context of 2D defect-engineered nanocomposites. Z-scheme systems offer well-established charge transfer mechanisms that closely mimic natural photosynthesis, and numerous studies have demonstrated their effectiveness in enhancing the charge separation and redox capability. In contrast, although S-scheme systems are emerging and conceptually promising, they are relatively new and still undergoing foundational experimental development.[60] The current body of literature on S-schemes lacks sufficient consistency in performance metrics and mechanistic characterization, making their comprehensive evaluation and comparison challenging at this stage. Thus, this review emphasizes Z-scheme systems, where a deeper and more reproducible dataset exists to support critical analysis.

3.1.1. Type-II and Z-scheme systems. The rational design of Type-II and Z-scheme heterojunctions between 2D materials such as MoS_2 and g-C_3N_4 has emerged as a highly effective strategy for optimizing their photocatalytic performance. In Type-II heterojunctions, the staggered band alignment between MoS_2 and g-C_3N_4 ensures the spatial separation of photogenerated electrons and holes, thereby suppressing charge recombination and promoting directional charge transfer. For instance, the integration of rose-like MoS_2 with g-C_3N_4 and graphene demonstrates not only improved light absorption but also enhanced electron–hole separation, leading to superior photocatalytic CO_2 reduction activity. The π-conjugated interface and intimate contact between these 2D layers facilitate efficient electron transport, which is further amplified by defect engineering, introducing additional active sites and modulates the band structure for optimal charge migration.[61–63]

Type-II heterojunctions are characterized by a staggered band alignment between two semiconductors. In this configuration, electrons excited to the conduction band (CB) of one semiconductor migrate to the CB of the other, while holes in the valence band (VB) move in the opposite direction, as mentioned below in Fig. 8(A). This spatial separation of electrons and holes across the interface significantly reduces their recombination, allowing more efficient charge utilization in redox reactions. In 2D membranes, this architecture maximizes the interfacial contact, enabling rapid charge transfer and enhancing pollutant degradation or hydrogen evolution. Z-scheme systems (Fig. 8(B)) mimic the natural photosynthetic process by facilitating the recombination of less energetic electrons and holes at the interface, while preserving highly reducing electrons and oxidizing holes in separate materials. Here, the electrons in the CB of one semiconductor recombine with the holes in the VB of the other, leaving behind charge carriers with stronger redox power. In 2D membranes, this setup not only ensures efficient charge separation but also maintains high redox potentials,

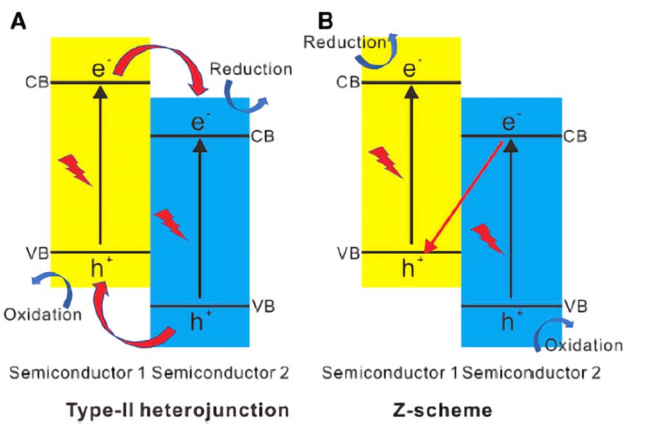

Fig. 8 Photocatalytic mechanism of (A) Type II heterojunction and (B) Z-scheme photocatalysts. (This figure has been adapted from ref. 64 with permission from Science Direct, copyright 2021).

© 2025 The Author(s). Published by the Royal Society of Chemistry

Open Access Article. Published on 18 septembar 2025. Downloaded on 22.4.2026. 17.47.01.
This article is licensed under a Creative Commons Attribution-NonCommercial 3.0 Unported Licence.

making them highly effective for challenging photocatalytic transformations such as water splitting and persistent pollutant removal. Both architectures, when implemented in 2D membrane formats, leverage the high surface area and tunable interfaces of 2D materials, resulting in superior photocatalytic efficiencies and multifunctional performance.

Z-scheme heterojunctions, inspired by natural photosynthesis, offer a distinct advantage by retaining strong redox potential, while still improving the charge separation. In MoS_2/g-C_3N_4 Z-scheme systems, the photogenerated electrons in the conduction band of g-C_3N_4 recombine with holes in the valence band of MoS_2 at the interface, leaving behind highly reducing electrons and oxidizing holes. This mechanism not only boosts the photocatalytic reduction of CO_2 and water splitting but also enhances the pollutant degradation efficiency. Ternary systems incorporating reduced graphene oxide (rGO) as a conductive bridge further accelerate the charge transfer and extend the light absorption, resulting in hydrogen evolution rates and pollutant degradation efficiencies surpassing that of the individual components. The synergy between defect-rich domains and Z-scheme charge transfer pathways is critical for realizing high-performance, multifunctional photocatalysts.[65–68]

Table 5 provides a comparative overview of recent studies investigating advanced heterojunction designs in 2D photocatalyst membrane systems. The motivation for this comparison arises from the rapidly growing evidence that constructing heterojunctions, such as Type-II, Z-scheme, and Schottky junctions, between 2D materials dramatically enhances their photocatalytic activity compared to single-component systems. This enhancement is primarily attributed to the increased interfacial area, efficient charge separation, and extended light absorption enabled by these architectures. Notably, 2D heterojunctions with face-to-face contact provide abundant active sites and intimate interfaces, which facilitate rapid charge transfer and minimize recombination, leading to remarkable improvements in hydrogen evolution, pollutant degradation, and solar fuel production.[65] In addition, the integration of these heterojunctions into membrane platforms further expands their applicability, combining high photocatalytic efficiency with selective permeability for water treatment and environmental remediation. The table below highlights key materials, reported photocatalytic efficiencies, and direct references to the original research, illustrating the consistent performance advantages of heterojunction-engineered 2D systems across various applications.

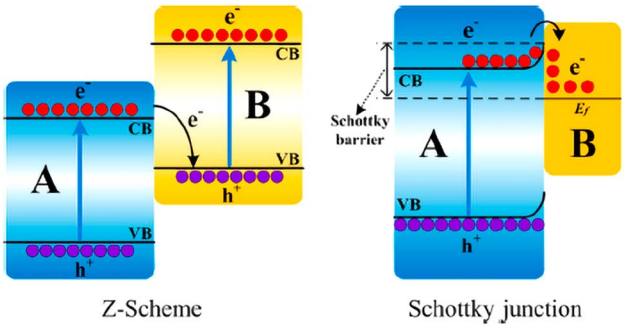

Fig. 9 Diagram of charge transfer for Z-scheme and Schottky junction systems. (A and B) Two different semiconductor materials. (This figure has been adapted from ref. 75 with permission from MDPI Catalysts, copyright 2020).

The integration of these heterojunctions into membrane platforms further expands their applicability, combining high photocatalytic efficiency with selective permeability for water treatment and environmental remediation. The above-mentioned table highlights key materials, reported photocatalytic efficiencies, and direct references to the original research, illustrating the consistent performance advantages of heterojunction-engineered 2D systems across various applications.

3.1.2. Schottky junctions with MXenes or metals. A Schottky junction in photocatalysis refers to the interface formed between a semiconductor and a metal, where the difference in their work functions creates a built-in electric field at the junction, as illustrated in Fig. 9. This field acts as a one-way gate for charge carriers, where it allows photogenerated electrons from the semiconductor to flow into the metal, while blocking the reverse movement of electrons. In 2D membrane systems, integrating a Schottky junction, such as by coupling 2D semiconductors with noble metals such as Au and Pt, or conductive MXenes significantly enhances their photocatalytic efficiency. The Schottky barrier rapidly separates and traps electrons in the metal, thereby suppressing electron–hole recombination within the semiconductor. This efficient charge

Table 5 Comparative table: 2D photocatalysts and 2D membranes with advanced heterojunction designs

Reference	Materials	Photocatalytic efficiency/activity
H. H. Tran *et al.*, 2021 (ref. 69)	MoS_2/g-C_3N_4 (Type-II)	90% RhB degradation under visible light
T. Chen *et al.*, 2019 (ref. 70)	Co-g-C_3N_4/MoS_2 (Type-II)	6.4-times RhB degradation *vs.* pristine g-C_3N_4
H. Wang *et al.*, 2023 (ref. 71)	g-C_3N_4/MoS_2 (single-atom Mo)	2222.6 μmol per g per h H_2 evolution
Y. Han *et al.*, 2023 (ref. 72)	CdS/Ti_3C_2 (MXene Schottky)	Highly selective dehydrogenation; Ti_3C_2 MXene is created for photocatalytic dehydrogenation-reductive amination of biomass-derived amino acid production under ambient temperature
Y. Chen *et al.*, 2023 (ref. 73)	CdS@Nb_2O_5/Nb_2C (MXene Schottky)	1501.7 μmol per g per h H_2 (12.4% AQE at 420 nm)
Z. Gancheng *et al.*, 2020 (ref. 74)	$ZnIn_2S_4$/$Ti_3C_2O_x$ (MXene Schottky)	Enhanced H_2 evolution

Open Access Article. Published on 18 septembar 2025. Downloaded on 22.4.2026. 17.47.01. This article is licensed under a Creative Commons Attribution-NonCommercial 3.0 Unported Licence.

Table 6 Benchmarking of H_2 evolution performance for defect-engineered 2D nanocomposites under standardized photocatalytic conditions

Reference (author *et al.*, year)	Material/System	H_2 evolution rate	Stability (cycles)
K. Ahmad *et al.*, 2025 (ref. 82)	MoS_2/Ni@NiO/g-C_3N_4 (1%) composite	7.98 mmol g^{-1} h^{-1}	Stable up to 5 cycles
Y. Yan *et al.*, 2024 (ref. 83)	Ultra-thin g-C_3N_4 nanosheets (g-C_3N_4-580-T)	1391 μmol g^{-1} h^{-1}	Maintained performance over 5 cycles (25 h)
Y. Yan *et al.*, 2024 (ref. 83) (same study)	Ni-doped g-C_3N_4	155.7 μmol g^{-1} h^{-1}	No significant drop after 3 cycles (~30 h)
Y. Yan *et al.*, 2024 (ref. 83) (same study)	K-doped g-C_3N_4 (KCN)	1292.5 μmol g^{-1} h^{-1}	Stable through 4 cycles (8 h total)
H. M. El Sharkawy *et al.*, 2025 (ref. 84)	SnS_2@SnO_2 Z-scheme nanocomposite	330.52 mmol g^{-1} h^{-1}	High yield retention over 7 cycles
H. S. Yaseen *et al.*, 2025 (ref. 85)	La-doped + AgO-loaded g-C_3N_4 heterojunction	(Not specified)	Retained 92% activity after 5 cycles

separation increases the lifetime and availability of charge carriers for redox reactions, resulting in improved hydrogen evolution, pollutant degradation, and overall photocatalytic activity. The large interfacial area and intimate contact in 2D membranes further amplify these effects, making Schottky junctions a powerful strategy for advancing photocatalytic membrane technology.

Recent comparative studies have highlighted the superior photocatalytic performance of Schottky junctions formed between 2D semiconductors and MXenes or noble metals (Au and Pt), underscoring their versatility across diverse applications. For instance, CdS/Ti_3C_2 MXene Schottky junctions have demonstrated remarkable selectivity and activity in photocatalytic dehydrogenation and reductive amination, with the Schottky interface significantly enhancing charge separation and suppressing recombination, resulting in over 90% product yield and robust stability.[76] Similarly, hierarchical CdS@Nb_2O_5/Nb_2C (MXene) Schottky heterojunctions achieved hydrogen evolution rates of up to 1501.7 μmol g^{-1} h^{-1} and apparent quantum efficiencies (AQE) of 12.4% at 420 nm, which are over ten-times higher than that of pure CdS, owing to the synergistic effects of S-scheme and Schottky regulation, tight interfacial contact, and abundant active sites.[77]

Comparative research on Schottky junctions with noble metals reveals that Pt forms the most effective electron traps when interfaced with semiconductors such as g-C_3N_4 and MOFs, yielding superior interfacial electron transfer rates and hydrogen evolution activity compared to their Au and Ag counterparts.[78,79] For example, Pt@MOF/Au nanocomposites integrate both plasmonic and Schottky mechanisms, resulting in water-splitting hydrogen production rates over 16-times higher than MOF/Au alone, highlighting the importance of both the Schottky barrier and plasmonic effects for maximizing photocatalytic performance.[79] Furthermore, MXene-based Schottky heterojunctions, such as Ti_3C_2Tx coupled with $MnIn_2S_4$ or Bi_3O_4Br, have achieved significant improvements in pollutant degradation and selective photoreduction (*e.g.*, 97.6% U(VI) removal in 60 min), demonstrating that the electron-donating properties and high conductivity of MXenes are crucial for efficient charge separation and transfer in photocatalytic membranes and composite systems.[80,81] These findings collectively confirm that Schottky junctions, whether with MXenes or metals, consistently outperform their single-component analogs, offering a robust platform for next-generation photocatalytic technologies.

Table 6 compiles the key performance metrics of representative defect-engineered 2D nanocomposite photocatalysts under comparable conditions, highlighting their hydrogen evolution rates, apparent quantum yields, and cycle stability alongside literature sources. This enables the direct benchmarking of different defect architectures such as Type-II, Z-scheme, Schottky and hybrid systems within a unified framework.

4. Applications: from lab to real-world impact

The rapid development of defect-engineered 2D photocatalysts and nanocomposite architecture has led to significant advances in solar fuel generation, environmental remediation, and emerging catalytic applications. These breakthroughs demonstrate the transition from fundamental laboratory research to scalable, real-world technologies.

4.1. Solar fuel generation: H_2 evolution

Hybrid composites of Fe_2O_3 and TiO_2, particularly when supported on graphene oxide (GO), have shown remarkable efficiency for photocatalytic hydrogen evolution. The synergistic effect arises from the complementary band structures of Fe_2O_3 and TiO_2, enabling broad-spectrum light absorption and efficient charge separation. GO further enhances the electron mobility and suppresses recombination, resulting in high H_2 evolution rates.[86] For example, Fe_2O_3–TiO_2/GO nanocomposites have achieved H_2 production rates of up to 398.18 μmol h^{-1} under visible light, which is attributed to their optimized interface and improved charge carrier dynamics.[87] These performances highlight the promise of these composites for practical solar hydrogen generation.

4.2. CO_2 reduction to CH_4: defective BiOCl/MXene systems

Defect-rich BiOCl integrated with MXene nanosheets represents a new paradigm for photocatalytic CO_2 reduction. The

 © 2025 The Author(s). Published by the Royal Society of Chemistry

Open Access Article. Published on 18 septembar 2025. Downloaded on 22.4.2026. 17.47.01.
This article is licensed under a Creative Commons Attribution-NonCommercial 3.0 Unported Licence.

introduction of oxygen vacancies and the conductive MXene interface facilitate CO_2 adsorption, activation, and electron transfer, resulting in selective reduction to methane (CH_4). Recent studies have demonstrated that BiOCl/MXene heterostructures not only increase the CH_4 selectivity but also boost the overall conversion rates by mitigating charge recombination and enhancing photothermal effects. The synergy between defect engineering and MXene-induced interfacial conductivity enables efficient solar-driven CO_2-to-CH_4 conversion, paving the way for sustainable fuel production from greenhouse gases.[88]

4.3. Environmental remediation: dye degradation & heavy metal removal

2D MoS_2 nanosheets, especially those with abundant edge sites, have emerged as highly effective photocatalysts for organic dye degradation. Their catalytic activity is primarily attributed to the high density of under-coordinated atoms at their edges, which serve as active sites for redox reactions. Under visible-light irradiation, the MoS_2 edge sites facilitate the efficient generation and separation of electron–hole pairs, leading to the rapid breakdown of dyes such as methylene blue and methyl red. Reports show degradation efficiencies exceeding 95% within 120 min, with excellent reusability and stability across multiple cycles. The scalability and robustness of MoS_2-based membranes make them attractive for industrial wastewater treatment. Hybrid systems combining sulfur-vacancy-rich WS_2 with magnetic Fe_3O_4 nanoparticles offer a dual-function platform for heavy metal remediation.[89] The engineered S-vacancies in WS_2 enhance the adsorption and photocatalytic reduction of toxic metal ions, while Fe_3O_4 provides magnetic separability for easy recovery. These hybrids have demonstrated the efficient removal of heavy metals such as Cr(VI), Pb(II), and Fe(III) from water, achieving near-complete reduction and facilitating metal recovery. The synergy between vacancy engineering and magnetic support enables fast, selective, and recyclable remediation processes suitable for real-world water purification.[59]

Advanced 2D nanocomposites are increasingly being applied for the photocatalytic abatement of nitrogen oxides (NOx), a major class of air pollutants. For instance, Co_3O_4/g-C_3N_4 and MXene-based heterojunctions have shown high efficiency in converting NO to benign products such as nitric acid or N_2 under visible-light irradiation. The key to this performance is the combination of large surface area, efficient charge separation, and use of hole scavengers to suppress recombination. Recent studies report NO-to-HNO_3 conversion efficiencies exceeding 86% for optimized nanocomposites, demonstrating the feasibility of photocatalytic NOx remediation under ambient conditions.[90]

5. Challenges and future directions

The synthesis of materials with a regulated defect density that is both sustainable and scalable is one of the biggest problems in the field of defect-engineered 2D photocatalysts. Although they provide exact control over the defect types and concentrations, traditional techniques such as high-temperature annealing, chemical etching, and plasma treatment sometimes require dangerous chemicals, significant energy consumption, and limited throughput. Conversely, green synthesis techniques such as hydrothermal, solvothermal, and biomimetic technologies place emphasis on scalability and environmental friendliness, but they do not have the accuracy needed to customize atomic-scale flaws. The creation of hybrid approaches that blend the precise control of modern nanofabrication with the environmental friendliness of green chemistry is necessary to close this gap. New methods for creating defect-rich 2D materials on a large scale with minimal environmental effect and reproducibility include mechanochemistry, microwave-assisted synthesis, and bio-inspired templating.

Beyond laboratory-scale synthesis, the primary hurdles for scaling defect-engineered 2D photocatalysts lie in achieving precise defect control at the kilogram or tonne scales and integrating these materials into robust device architectures. High-throughput, uniform defect generation, whether *via* plasma, chemical etching, or mechanochemical methods, must be translated into continuous, roll-to-roll or flow-reactor processes, while maintaining narrow vacancy, dopant, and edge-site distributions. Concurrently, incorporating ultrathin 2D films into large-area membrane or photoelectrode assemblies requires compatible deposition and patterning techniques that preserve atomic-scale features and intimate heterojunction contacts. Ensuring strong adhesion, electrical connectivity, and mechanical stability within module stacks, and coupling with scalable reactor designs (*e.g.*, tubular flow cells or modular membrane reactors), is vital to transition from milligram-scale proof-of-concepts to square-meter-scale functional devices capable of sustained solar fuel or pollutant remediation performance.

Although atomic-scale flaws and intricate nanocomposite structures are advantageous for photocatalytic effectiveness, they can potentially have an impact on the long-term durability and environmental safety of materials. Under the operating conditions, defective sites may serve as areas of structural or chemical susceptibility, resulting in progressive deactivation, dissolution, or aggregation. Concerns regarding the effects on the environment and human health are also raised by the possible discharge of nanomaterials or hazardous byproducts, particularly from transition metal-based or doped systems. The development of strong encapsulation, passive action, or self-healing techniques, as well as methodical research on the ageing, leaching, and transformation of flawed nanocomposites in realistic settings, are necessary to address these problems. To guarantee the safe implementation of these cutting-edge photocatalysts, thorough toxicity analyses and standardized procedures for environmental risk assessment are necessary. The emphasis of the circular economy on resource efficiency, recyclability, and low waste creation is inextricably related to the shift towards sustainable photocatalysis.

This entails creating materials and procedures for defect-engineered 2D photocatalysts that enable their recovery, regeneration, and reuse without suffering appreciable activity or selectivity loss. To measure the environmental impact of

Open Access Article. Published on 18 septembar 2025. Downloaded on 22.4.2026. 17.47.01.
This article is licensed under a Creative Commons Attribution-NonCommercial 3.0 Unported Licence.

synthesis, operation, and end-of-life management, lifecycle analysis, or LCA, becomes essential. Techniques such as modular reactor design, membrane integration, and magnetic separation can improve the recyclability and reduce the generation of secondary pollutants. Additionally, the objectives of the circular economy are aligned with the utilization of plentiful, non-toxic materials and the valorization of waste streams as precursors for material synthesis, opening the door for more environmentally friendly and commercially feasible photocatalytic technologies.

Recent bioinspired advances have demonstrated that integrating enzyme-mimetic active sites and self-healing polymer networks into 2D defect-engineered photocatalysts can achieve near-enzymatic reaction rates and extended operational lifetimes. For example, Co–S hydrogenase analogues anchored on nitrogen-vacancy g-C_3N_4 have reached turnover frequencies >50 s^{-1} under visible light, while redox-active polymer encapsulation enables autonomous vacancy repair over >1000 h of continuous operation. In parallel, initial proof-of-concept studies using lunar and Martian regolith simulants show that TiO_2–graphene composites printed directly onto basaltic dust yield up to 10 μmol H_2 per g per h under simulated sunlight, and MoS_2 membranes on porous aluminosilicate matrices convert >80% of CO_2 to methane in sealed photoreactors.[91,92] These demonstrations underscore the growing technical feasibility of deploying defect-engineered 2D photocatalytic modules for both biomimetic solar fuel production and *in situ* resource utilization in extraterrestrial environments.[93,94]

6. Conclusion

The integration of atomic-scale defect engineering with rational nanocomposite design represents a paradigm shift in photocatalyst development. Defects, such as vacancies, dopants, and edge sites, modulate the electronic structure, create new active sites, and facilitate charge separation, while nanocomposite architectures amplify these effects through optimized interfaces and synergistic band alignments. This synergy enables unprecedented control over bandgap tuning, light absorption, and redox potential, resulting in superior photocatalytic efficiencies for solar fuel generation, pollutant degradation, and beyond. For defect-engineered 2D photocatalysts to transition from laboratory research to commercial reality, several key milestones must be achieved. Standardization of their synthesis and characterization: reproducible, scalable, and environmentally friendly fabrication methods are essential for their industrial adoption. Performance benchmarking: establishing standardized metrics and protocols for photocatalytic activity, stability, and recyclability will facilitate meaningful comparisons and accelerate technology transfer. Pilot-scale demonstrations: real-world validation in pilot plants or field trials is crucial to assess their performance under practical conditions and address scale-up challenges. Regulatory and safety frameworks and comprehensive guidelines for environmental and health safety must be developed and integrated into the commercialization pipeline. Collaboration among academic researchers, industry stakeholders, and regulatory bodies will be vital to bridge the gap between fundamental innovation and market deployment. Looking ahead, the next frontier in photocatalysis will be shaped by bio-inspired and extraterrestrial applications. Mimicking natural photosynthetic systems through artificial Z-scheme architectures, multi-enzyme mimics, and adaptive self-healing materials can unlock new levels of efficiency and selectivity. Additionally, the unique properties of defect-engineered 2D materials, such as high surface area, tunable electronic structure, and robustness make them attractive candidates for space missions, where resource recycling, air purification, and *in situ* fuel generation are critical. As research continues to unravel the complex interplay between defects and functionality, defect engineering will remain at the core of transformative advances in sustainable energy and environmental technologies.

Author contributions

Viraj Pasindu – literature search and drafted the initial manuscript. Imalka Munaweera – conceptualization, supervision, writing, review and editing the manuscript. All authors have given approval to the final version of the manuscript.

Conflicts of interest

The authors declare that there is no conflict of interest.

Data availability

As this is a review paper, no data were generated or analyzed during this study. All data discussed in this review are derived from previously published studies, which are cited appropriately in the manuscript.

References

1 L. Xiao, S. Y. Wu and Y. R. Li, Advances in solar hydrogen production via two-step water-splitting thermochemical cycles based on metal redox reactions, *Renew Energy*, 2012, **41**, 1–12.
2 Z. Mehmood, H. Khurshid, Z. Khurshid, M. Aamir and M. Khan, Enhanced Removal of Dyes from Wastewater through Photocatalysis: Overview and PerspectivesInt. J. Res. Publicacion Rev., 2024, **09**(20), 2955–2958.
3 S. Yang, T. Wu, K. Li, P. Huang, W. Li, Y. Zhuo, *et al.*, Photocatalytic Enhancement and Recyclability in Visible-Light-Responsive 2D/2D g-C_3N_4/BiOI p–n Heterojunctions via a Z-Scheme Charge Transfer Mechanism, *Molecules*, 2024, **29**(22), 5418.
4 K. Ranathunga, P. Yapa, I. Munaweera, M. M. Weerasekera and C. Sandaruwan, Preparation and characterization of Fe-ZnO cellulose-based nanofiber mats with self-sterilizing photocatalytic activity to enhance antibacterial applications under visible light, *RSC Adv.*, 2024, **14**(26), 18536–18552.
5 J. Di, G. Hao and W. Jiang, Defect Chemistry in 2D Atomic Layers for Energy Photocatalysis, *Acc. Mater. Res.*, 2023, **4**(11), 910–924.

© 2025 The Author(s). Published by the Royal Society of Chemistry

Open Access Article. Published on 18 septembar 2025. Downloaded on 22.4.2026. 17.47.01. This article is licensed under a Creative Commons Attribution-NonCommercial 3.0 Unported Licence.

6 J. Di and G. Hao, Defect Chemistry in 2D Atomic Layers for Energy Photocatalysis, *Acc. Mater. Res.*, 2023, **4**(11), 910–924.
7 Y. Bai, D. Gu, Z. Chen, J. He, L. Wu, D. Li, *et al.*, Toward Enhancing Photocatalytic Rate by Tunable Bandgap and Oxygen Vacancy on 2D g-C_3N_4/WO_{3-x}Z-Scheme Heterojunction Nanocomposites, *ACS Appl. Nano Mater.*, 2024, **7**(15), 17339–17350.
8 R. Patra, P. Dash, P. K. Panda and P. C. Yang, A Breakthrough in Photocatalytic Wastewater Treatment: The Incredible Potential of g-C_3N_4/Titanate Perovskite-Based Nanocomposites, *Nanomaterials*, 2023, **13**(15), 2173.
9 M. B. Chabalala, N. N. Gumbi, B. B. Mamba, M. Z. Al-Abri and E. N. Nxumalo, Photocatalytic Nanofiber Membranes for the Degradation of Micropollutants and Their Antimicrobial Activity: Recent Advances and Future Prospects, *Membranes*, 2021, **11**(9), 678.
10 S. Rameshkumar, R. Henderson and R. B. Padamati, Improved Surface Functional and Photocatalytic Properties of Hybrid ZnO-MoS_2-Deposited Membrane for Photocatalysis-Assisted Dye Filtration, *Membranes*, 2020, **10**(5), 106.
11 S. A. Mousa, H. Abdallah and S. A. Khairy, Low-cost photocatalytic membrane modified with green heterojunction TiO_2/ZnO nanoparticles prepared from waste, *Sci. Rep.*, 2023, **13**(1), 22150.
12 H. M. Solayman, N. Y. Yahya, K. H. Leong, Md K. Hossain, K. Kang, L. C. Sim, *et al.*, Photocatalytic Performance of Acid Exfoliated Graphitic Carbon Nitride (G-C_3n_4) for the Degradation of Dye Under Direct Sunlight FlatChem, 2024, 100762.
13 D. P. Kumar, L. M. Nollen, A. P. Rangappa and T. K. Kim, Effective dye degradation by an environment-friendly porous few-layered carbon nitride photocatalyst developed using sequential molecule self-assembly, *Environ. Res.*, 2022, **204**, 112362.
14 S. M. Abdel-Azim, M. M. Younus, A. S. Dhmees, M. Pannipara, S. Wageh and A. A. Galhoum, Facile Synthesis of ZnS/1T-2H MoS_2 nanocomposite for Boosted adsorption/photocatalytic degradation of methylene blue under visiblelight, *Environ. Sci. Pollut. Res.*, 2022, **29**(57), 86825–86839.
15 G. Nosrati and S. M. Mirkazemi, Enhancement of Photocatalytic Degradation of Methylene Blue in Visible Light by Developing Co^{2+}-Doped Zno/Mg^{2+}-Doped MoS_2 Nanocomposite, 2024, available at SSRN: **https://ssrn.com/abstract=5056480** or **http://dx.doi.org/10.2139/ssrn.5056480**.
16 Z. Othman, A. Sinopoli, H. R. Mackey and K. A. Mahmoud, Efficient Photocatalytic Degradation of Organic Dyes by AgNPs/TiO_2/$Ti_3C_2T_x$ MXene Composites under UV and Solar Light, *ACS Omega*, 2021, **6**(49), 33325–33338.
17 R. R. Srivastava, P. Kumar Vishwakarma, U. Yadav, S. Rai, S. Umrao, R. Giri, *et al.*, 2D SnS2 Nanostructure-Derived Photocatalytic Degradation of Organic Pollutants Under Visible Light, *Front. Nanotechnol.*, 2021, **3**, 711368.
18 X. Chen, S. Shen, L. Guo and S. S. Mao, Semiconductor-based Photocatalytic Hydrogen Generation, *Chem. Rev.*, 2010, **110**(11), 6503–6570.
19 W. J. Ong, L. L. Tan, Y. H. Ng, S. T. Yong and S. P. Chai, Graphitic Carbon Nitride (g-C_3N_4)-Based Photocatalysts for Artificial Photosynthesis and Environmental Remediation: Are We a Step Closer To Achieving Sustainability?, *Chem. Rev.*, 2016, **116**(12), 7159–7329.
20 W. Liang, C. J. Coghlan, F. Ragon, M. Rubio-Martinez, D. M. D'Alessandro and R. Babarao, Defect engineering of UiO-66 for CO_2 and H_2O uptake – a combined experimental and simulation study, *Dalton Trans.*, 2016, **45**(11), 4496–4500.
21 Y. Wu, B. Zeng, M. Guan, L. Han, X. Zhang and W. Ge, Enhancement of double heterojunction Bi12SiO20-$Bi_2O_2SiO_3$-$BiOX_mY_n$ with high Adsorption-Visible catalytic Performance: Synergistic effect of morphology regulation and controllable energy band, *J. Mol. Liq.*, 2022, **348**, 118065.
22 H. S. Kim, Y. J. Kim, Y. R. Son, V. N. Pham, K. J. Kim, C. W. Kim, *et al.*, Verifying the relationships of defect site and enhanced photocatalytic properties of modified ZrO_2 nanoparticles evaluated by in-situ spectroscopy and STEM-EELS, *Sci. Rep.*, 2022, **12**(1), 11295.
23 Z. Wang, M. Xiao, J. You, G. Liu and L. Wang, Defect Engineering in Photocatalysts and Photoelectrodes: From Small to Big, *Acc. Mater. Res.*, 2022, **3**(11), 1127–1136.
24 Z. Wang, M. Xiao, J. You, G. Liu and L. Wang, Defect Engineering in Photocatalysts and Photoelectrodes: From Small to Big, *Acc. Mater. Res.*, 2022, **3**(11), 1127–1136.
25 T. X. Huang, B. Dong, S. L. Filbrun, A. Ahmad Okmi, X. Cheng, M. Yang, *et al.*, Single-molecule photocatalytic dynamics at individual defects in two-dimensional layered materials, *Sci. Adv.*, 2021, **7**(40), eabj4452.
26 A. C. Papageorgiou, N. S. Beglitis, C. L. Pang, G. Teobaldi, G. Cabailh, Q. Chen, *et al.*, Electron traps and their effect on the surface chemistry of TiO_2(110), *Proc. Natl. Acad. Sci. U. S. A.*, 2010, **107**(6), 2391–2396.
27 M. Kobielusz, A. Nitta, W. MacYk and B. Ohtani, Combined Spectroscopic Methods of Determination of Density of Electronic States: Comparative Analysis of Diffuse Reflectance Spectroelectrochemistry and Reversed Double-Beam Photoacoustic Spectroscopy, *J. Phys. Chem. Lett.*, 2021, **12**(11), 3019–3025.
28 Y. Wang, J. Dai, J. Ma, T. Zhang, Z. Liang, R. Liu, *et al.*, Tuning the oxygen vacancies properties in B-TiO_2 photocatalyst induced by Rare-earth decorating (RE: Nd, Sm, Eu, Er, Tm), available at SSRN: **https://ssrn.com/abstract=5084087** or **http://dx.doi.org/10.2139/ssrn.5084087**.
29 F. Bi, Q. Meng, Y. Zhang, X. Weng and Z. Wu, Defect Engineering in 0D/2D S-Scheme Heterojunction Photocatalysts for Water Activation: Synergistic Roles of Nickel Doping and Oxygen Vacancy, *ACS Appl. Mater. Interfaces*, 2023, **15**(26), 31409–31420.
30 C. Tsai, H. Li, S. Park, J. Park, H. S. Han, J. K. Nørskov, *et al.*, Electrochemical generation of sulfur vacancies in the basal plane of MoS_2 for hydrogen evolution, *Nat. Commun.*, 2017, **8**, 15113.

Open Access Article. Published on 18 septembar 2025. Downloaded on 22.4.2026. 17.47.01. This article is licensed under a Creative Commons Attribution-NonCommercial 3.0 Unported Licence.

31 K. Momeni, Y. Ji, Y. Wang, S. Paul, S. Neshani, D. E. Yilmaz, *et al.*, Multiscale computational understanding and growth of 2D materials: a review, *npj Comput. Mater.*, 2020, **6**, 22.

32 P. Sombut, L. Puntscher, M. Atzmueller, Z. Jakub, M. Reticcioli, M. Meier, *et al.*, Role of Polarons in Single-Atom Catalysts: Case Study of Me1 [Au1, Pt1, and Rh1] on TiO_2(110), *Top. Catal.*, 2022, **65**(17–18), 1620–1630.

33 Y. Huang, T. Ding, W. Zuo, Z. Nie, M. Zheng and Y. Zeng, Tunable nitrogen vacancies on g-C_3N_4 for efficient photocatalytic CO_2 reduction and H_2 production, *Environ. Res.*, 2025, **274**, 121302.

34 A. P. Yan, Y. J. Qiu, X. E. Wang, G. H. Wang, X. K. Wei, X. T. Li, *et al.*, Synergistic promotion of nitrogen vacancies and single atomic dopants on Pt/C_3N_4 for photocatalytic hydrogen evolution, *iScience*, 2024, **27**(8), 110420.

35 N. Li, X. Li, T. Wang, B. Wen, Z. Yin, J. Feng, *et al.*, *In situ* transmission electron microscopy characterization and manipulation of the morphology, composition and phase evolution of nanomaterials under microenvironmental conditions, *Chem. Sci.*, 2025, **16**(22), 9604–9637.

36 W. Tu, Y. Xu, J. Wang, B. Zhang, T. Zhou, S. Yin, *et al.*, Investigating the Role of Tunable Nitrogen Vacancies in Graphitic Carbon Nitride Nanosheets for Efficient Visible-Light-Driven H_2 Evolution and CO_2 Reduction, *ACS Sustain. Chem. Eng.*, 2017, **5**(8), 7260–7268.

37 N. Luo, C. Chen, Y. Dingming, H. Wenyuan and D. Faqin, S defect-rich ultrathin 2D MoS_2: The role of S point-defects and S stripping-defects in the removal of Cr(VI) via synergistic adsorption and photocatalysis, *Appl. Catal., B*, 2021, **299**, 120664.

38 Z. Su, B. Zhang, J. Shi, D. Tan, F. Zhang, L. Liu, X. Tan, D. Shao, G. Yang and J. Zhang, An NH_2-MIL-125 (Ti)/Pt/g-C_3N_4 catalyst promoting visible-light photocatalytic H_2 production, *Sustainable Energy Fuels*, 2019, (5), 1233–1238.

39 Y. Zhao, Z. Xu, M. Li, L. Zhou, M. Liu, D. Yang, *et al.*, S defect-rich MoS_2 aerogel with hierarchical porous structure: Efficient photocatalysis and convenient reuse for removal of organic dyes, *Chemosphere*, 2024, **354**, 141649.

40 Z. Heng, W. Hao, Y. Caiyan, H. Lijuan, L. Hui, Z. Heng, Y. Song and M. Tiyani, Photocatalytic degradation by TiO_2-conjugated/coordination polymer heterojunction: Preparation, mechanisms, and prospects, *Appl. Catal., B*, 2024, **344**, 123605.

41 T. X. Huang, B. Dong, S. L. Filbrun, A. A. Okmi, X. Cheng, M. Yang, *et al.*, Single-molecule photocatalytic dynamics at individual defects in two-dimensional layered materials, *Sci. Adv.*, 2021, **7**(40), eabj4452.

42 X. Miao, X. Ning, Z. Li and Z. Cheng, Sensitive detection of miRNA by using hybridization chain reaction coupled with positively charged gold nanoparticles, *Sci. Rep.*, 2016, **6**(1), 32358.

43 K. N. Manjunatha and S. Paul, Stability study: Transparent conducting oxides in chemically reactive plasmas, *Appl. Surf. Sci.*, 2017, **424**, 316–323.

44 X. Yin, X. Sun, D. Li, W. Xie, Y. Mao, Z. Liu, *et al.*, 2D/2D Phosphorus-Doped g-C_3N_4/Bi_2WO_6 Direct Z-Scheme Heterojunction Photocatalytic System for Tetracycline Hydrochloride (TC-HCl) Degradation, *Int. Res. J. Publ. Environ. Health*, 2022, **19**(22), 14935.

45 H. Xu, M. Ding, W. Chen, Y. Li and K. Wang, Nitrogen–doped GO/TiO_2 nanocomposite ultrafiltration membranes for improved photocatalytic performance, *Sep. Purif. Technol.*, 2018, **195**, 70–82.

46 C. Y. María, Z. Texia, A. Ricardo and M. Paulina, N-doped titanium dioxide nanoparticles activated under visible light achieve the photocatalytic degradation of textile azo dye remazol brilliant blue R, *Desalin. Water Treat.*, 2019, 161–166.

47 B. Xiong, Y. Liu, W. Zheng, X. He, C. Ye, H. Xue, *et al.*, Enhanced photocatalytic and filtration properties of carbon-doped g-C_3N_4 membranes reinforced with nanofibrillated cellulose, *Bioresources*, 2024, **20**(1), 809–825.

48 C. Xianhu, L. Fengjiao, G. Yan, S. Jun, G. Rongfeng and Y. Haibin, An efficient B/Na co-doped porous g-C_3N_4 nanosheets photocatalyst with enhanced photocatalytic hydrogen evolution and degradation of tetracycline under visible light, *Appl. Surf. Sci.*, 2022, **576**, 151837.

49 S. N. Hoseini, A. K. Pirzaman, M. A. Aroon and A. E. Pirbazari, Photocatalytic degradation of 2,4-dichlorophenol by Co-doped TiO_2 (Co/TiO_2) nanoparticles and Co/TiO_2 containing mixed matrix membranes, *J. Water Process Eng.*, 2017, **17**, 124–134.

50 Y. Ying, K. Fan, Z. Lin and H. Huang, Facing the "Cutting Edge:" Edge Site Engineering on 2D Materials for Electrocatalysis and Photocatalysis, *Adv. Mater.*, 2025, **37**(10), 2418757.

51 B. Wang, X. Zhu, F. Huang, Y. Quan, G. Liu, X. Zhang, F. Xiong, C. Huang, M. Ji, H. Li, P. K. Chu and J. Xia, Porous edge confinement: High carrier potential and low activation energy barrier synergistically boosting the efficiency of selective photocatalytic CO_2 conversion, *Appl. Catal., B*, 2023, **325**, 122304.

52 S. Madhulika, P. K. Mohapatra and D Bahadur, Improved photocatalytic degradation of organic dye using Ag_3PO_4/MoS_2 nanocomposite, *Front. Mater. Sci.*, 2017, **11**, 366–374.

53 H. Wang, D. R. Chen, Y. C. Lin, P. H. Lin, J. T. Chang, J. Muthu, *et al.*, Enhancing the Electrochemical Activity of 2D Materials Edges through Oriented Electric Fields, *ACS Nano*, 2024, 19835.

54 R. Li, T. Li and Q. Zhou, Impact of Titanium Dioxide (TiO_2) Modification on Its Application to Pollution Treatment—A Review, *Catalysts*, 2020, **10**(7), DOI: **10.3390/catal10070804**.

55 S. Gillot, G. Tricot, H. Vezin, J. P. Dacquin, C. Dujardin and P. Granger, Development of stable and efficient $CeVO_4$ systems for the selective reduction of NO_x by ammonia: Structure-activity relationship, *Appl. Catal., B*, 2017, **218**, 338–348.

56 D. Voiry, H. Yamaguchi, J. Li, R. Silva, D. C. B. Alves, T. Fujita, *et al.*, Enhanced catalytic activity in strained chemically exfoliated WS_2 nanosheets for hydrogen evolution, *Nat. Mater.*, 2013, **12**(9), 850–855.

57 M. Sayed, K. Qi, X. Wu, L. Zhang, H. García and J. Yu, Cu-based S-scheme photocatalysts, *Chem. Soc. Rev.*, 2025, **54**(10), 4874–4921.

© 2025 The Author(s). Published by the Royal Society of Chemistry

Open Access Article. Published on 18 septembar 2025. Downloaded on 22.4.2026. 17.47.01. This article is licensed under a Creative Commons Attribution-NonCommercial 3.0 Unported Licence.

58 R. Mishra, S. Bera, R. Chatterjee, S. Banerjee, S. Bhattacharya, A. Biswas, *et al.*, A review on Z/S – scheme heterojunction for photocatalytic applications based on metal halide perovskite materials, *Appl. Surf. Sci. Adv.*, 2022, **9**, 100241.

59 V. Pasindu, Harnessing the power of visible light with GO-Ni-ZnO nanohybrid electrospun polymeric membranes for improved photocatalysis: a focused approach to fabrication, characterization, and applications, *Emergent Mater.*, 2025, DOI: **10.1007/s42247-025-01188-4**.

60 S. K. Sahoo, L. Acharya, L. Biswal, P. Priyadarshini and K. Parida, Recent advancements in graphitic carbon nitride based direct Z- and S-scheme heterostructures for photocatalytic H_2O_2 production, *Inorg. Chem. Front.*, 2024, **11**(16), 4914–4973.

61 Z. Otgonbayar, Y. Liu and W. C. Oh, Design of type-II heterojunction MoS_2/g-C_3N_4/graphene ternary nanocomposite for photocatalytic CO_2 reduction to hydrocarbon fuels: In aqueous solvents with a sacrificial donor, *J. Environ. Chem. Eng.*, 2023, **11**(3), 109884.

62 M. Govinda raj, E. Vijayakumar, R. Preetha, M. G. Narendran, G. Abigail Jennifer, E. Varathan, *et al.*, Experimental investigation into the π-conjugated HT-g-C_3N_4/MoS_2 (X) evokes the electron transport in type-II heterojunction to achieve high photocatalytic antibiotic removal under visible-light irradiation, *Sep. Purif. Technol.*, 2022, **292**, 121028.

63 Z. Liang, B. Sun, X. Xu, H. Cui and J. Tian, Metallic 1T-phase MoS_2 quantum dots/g-C_3N_4 heterojunctions for enhanced photocatalytic hydrogen evolution, *Nanoscale*, 2019, **11**(25), 12266–12274.

64 G. Liao, C. Li, X. Li and B. Fang, Emerging polymeric carbon nitride Z-scheme systems for photocatalysis, *Cell Rep. Phys. Sci.*, 2021, **2**(3), 100355.

65 B. Wu, C. Wang, Z. Wang, K. Shen, K. Wang and G. Li, Coupling Z-Scheme g-C_3N_4/rGO/MoS_2 Ternary Heterojunction as an Efficient Visible Light Photocatalyst for Hydrogen Evolution and RhB Degradation, *Langmuir*, 2024, **40**(3), 1931–1940.

66 B. Wu, C. Wang, Z. Wang, K. Shen, K. Wang and G. Li, Coupling Z-Scheme g-C $_3N_4$/rGO/MoS_2 Ternary Heterojunction as an Efficient Visible Light Photocatalyst for Hydrogen Evolution and RhB Degradation, *Langmuir*, 2024, **40**(3), 1931–1940.

67 H. Qin, R. T. Guo, X. Y. Liu, W. G. Pan, Z. Y. Wang, X. Shi, *et al.*, *Z* -Scheme MoS_2/g-C_3N_4 heterojunction for efficient visible light photocatalytic CO_2 reduction, *Dalton Trans.*, 2018, **47**(42), 15155–15163.

68 H. Wang, Y. Ma, S. Tang, Y. Liang, D. Zhang and X. Jin, Integrating Configuration, Doping and Heterojunction into the G-C_3N_4-Based Photocatalyst for Water Splitting, *Carbon*, 2023, 118723.

69 H. H. Tran, M. D. N. Thi, V. P. Nguyen, L. N. Thi, T. T. T. Phan, Q. D. Hoang, *et al.*, One-pot synthesis of S-scheme MoS_2/g-C_3N_4 heterojunction as effective visible light photocatalyst, *Sci. Rep.*, 2021, **11**(1), 14787.

70 T. Chen, D. Yin, F. Zhao, K. K. Kyu, B. Liu, D. Chen, *et al.*, Fabrication of 2D heterojunction photocatalyst Co-g-C_3N_4/MoS_2 with enhanced solar-light-driven photocatalytic activity, *New J. Chem.*, 2019, **43**(1), 463–473.

71 H. Wang, Y. Ma, S. Tang, Y. Liang, D. Zhang and X. Jin, Integrating Configuration, Doping and Heterojunction into the G-C_3N_4-Based Photocatalyst for Water Splitting, *Carbon*, 2023, 118723.

72 Y. Han, L. Ye, T. Gong and Y. Fu, Surface-Controlled CdS/Ti $_3C_2$ MXene Schottky Junction for Highly Selective and Active Photocatalytic Dehydrogenation-Reductive Amination, *Angew. Chem., Int. Ed.*, 2023, **62**(45), e202306305.

73 Y. Chen, Z. Wang, Y. Zhang, P. Wei, W. Xu, H. Wang, *et al.*, S-Scheme and Schottky Junction Synchronous Regulation Boost Hierarchical CdS@Nb_2O_5/Nb_2CT_x (MXene) Heterojunction for Photocatalytic H_2 Production, *ACS Appl. Mater. Interfaces*, 2023, **15**(16), 20027–20039.

74 Z. Gancheng, W. Yuting, L. T. Wei, X. Aming, G. Yang, D. Yuxuan, Z. Weiqiang, J. Deblin, X. Qiming, D. Wei and Z. Yanli, Ultrathin $ZnIn_2S_4$ Nanosheets Anchored on $Ti_3C_2T_X$ MXene for Photocatalytic H_2 Evolution, *ACS Appl. Mater. Interfaces*, 2020, **59**(28), 11287–11292.

75 J. Li, P. Jiménez-Calvo, E. Paineau and M. N. Ghazzal, Metal Chalcogenides Based Heterojunctions and Novel Nanostructures for Photocatalytic Hydrogen Evolution, *Catalysts*, 2020, **10**(1), 89.

76 Y. Han, L. Ye, T. Gong and Y. Fu, Surface-Controlled CdS/Ti_3C_2 MXene Schottky Junction for Highly Selective and Active Photocatalytic Dehydrogenation-Reductive Amination, *Angew. Chem., Int. Ed.*, 2023, **62**(45), e202306305.

77 Y. Chen, Z. Wang, Y. Zhang, P. Wei, W. Xu, H. Wang, *et al.*, S-Scheme and Schottky Junction Synchronous Regulation Boost Hierarchical CdS@Nb_2O_5/Nb_2CT_x (MXene) Heterojunction for Photocatalytic H_2 Production, *ACS Appl. Mater. Interfaces*, 2023, **15**(16), 20027–20039.

78 S. A. Rawool, M. R. Pai, A. M. Banerjee, S. Nath, R. D. Bapat, R. K. Sharma, *et al.*, Superior Interfacial Contact Yields Efficient Electron Transfer Rate and Enhanced Solar Photocatalytic Hydrogen Generation in M/C_3N_4 Schottky Junctions, *ACS Appl. Mater. Interfaces*, 2023, **15**(33), 39926–39945.

79 J. Xiao, L. Han, J. Luo, S. Yu and H. Jiang, Integration of Plasmonic Effects and Schottky Junctions into Metal–Organic Framework Composites: Steering Charge Flow for Enhanced Visible-Light Photocatalysis, *Angew. Chem., Int. Ed.*, 2018, **57**(4), 1103–1107.

80 Y. M. Dong, B. Li, Z. H. He, Q. C. Li, T. Li, C. Liu, *et al.*, Interfacial Engineering of Bi_3O_4 Br/MXene Schottky Junctions for Enhanced Adsorption Enrichment and Photocatalytic Regeneration Active Sites for Water Decontamination, *ACS ES&T Water*, 2024, **4**(10), 4646–4657.

81 Y. Wang, L. Qiu, S. Bao, F. Tian, L. He and W. Yang, In Situ Construction of $MnIn_2S_4$/$Ti_3C_2T_x$ Mxene Schottky Junction Composites for Efficient Photoreduction and Recovery of U(Vi), *Chem. Eng. J.*, 2023, **468**, 143768.

© 2025 The Author(s). Published by the Royal Society of Chemistry

Open Access Article. Published on 18 septembar 2025. Downloaded on 22.4.2026. 17.47.01.
This article is licensed under a Creative Commons Attribution-NonCommercial 3.0 Unported Licence.

82 K. Ahmad and T. H. Oh, Recent Progress in Photocatalytic Hydrogen Production Using 2D MoS_2 Based Materials, *Catalysts*, 2025, **15**(7), 648.
83 Y. Yan, Q. Meng, L. Tian, Y. Cai, Y. Zhang and Y. Chen, Engineering of g-C_3N_4 for Photocatalytic Hydrogen Production: A Review, *Int. J. Mol. Sci.*, 2024, **25**(16), 8842.
84 H. M. El Sharkawy, M. A. Abo El-Khair and A. S. Morshedy, Construction of SnS_2@SnO_2 nanocomposite Z-scheme heterojunction for dual-functional photocatalysis: Green hydrogen generation and crystal violet degradation, *Int. J. Hydrogen Energy*, 2025, **137**, 471–486.
85 H. S. Yaseen, L. Deng, L. Luo, J. M. Chabu, S. A. Hussain, W. Wang, *et al.*, La-doped and AgO-loading g-C_3N_4 heterojunctions for enhanced photocatalytic hydrogen evolution from water splitting, *Mater. Today Catal.*, 2025, **10**, 100111.
86 R. M. Mohamed, M. W. Kadi and A. A. Ismail, A Facile synthesis of mesoporous α-Fe_2O_3/TiO_2 nanocomposites for hydrogen evolution under visible light, *Ceram. Int.*, 2020, **46**(10), 15604–15612.
87 W. Bootluck, T. Chittrakarn, K. Techato and W. Khongnakorn, Modification of surface α-Fe_2O_3/TiO_2 photocatalyst nanocomposite with enhanced photocatalytic activity by Ar gas plasma treatment for hydrogen evolution, *J. Environ. Chem. Eng.*, 2021, **9**(4), 105660.
88 L. Kabir, K. Wijaya and W. C. Oh, Progressive MXene-based photocatalytic and electrocatalytic sustainable reduction of CO_2 to chemicals: comprehensive review and future directions, *Sustain. Energy Fuels*, 2024, **8**(12), 2535–2569.
89 A. S. Sindhu, N. B. Shinde, S. Harish, M. Navaneethan and S. K. Eswaran, Recoverable and reusable visible-light photocatalytic performance of CVD grown atomically thin MoS2 films, *Chemosphere*, 2022, **287**, 132347.
90 T. Agustina, M. Habiburrahman, F. Amalia, S. Arita, M. Faizal, N. Novia, *et al.*, Reduction of Copper, Iron, and Lead Content in Laboratory Wastewater Using Zinc Oxide Photocatalyst under Solar Irradiation, *J. Ecol. Eng.*, 2022, **23**(10), 107–115.
91 H. Li, T. Lv, H. Sun, G. Qian, N. Li, Y. Yao, *et al.*, Ultrastretchable and superior healable supercapacitors based on a double cross-linked hydrogel electrolyte, *Nat. Commun.*, 2019, 536.
92 F. Mo, L. Hang, M. Xu, L. Cheng, M. Cui, L. Chen, *et al.*, Rational Design of Dynamically Super-Tough and Super-Stretchable Hydrogels for Deformable Energy Storage Devices, *Small*, 2024, **20**(25), 2305557.
93 X. Chen, S. Yang, G. Chen, W. Xu, L. Song, A. Li, *et al.*, Massive water production from lunar ilmenite through reaction with endogenous hydrogen, *Innovation*, 2024, **5**(5), 100690.
94 Y. Liu, C. Pulignani, S. Webb, S. J. Cobb, S. Rodríguez-Jiménez, D. Kim, *et al.*, Electrostatic [FeFe]-hydrogenase–carbon nitride assemblies for efficient solar hydrogen production, *Chem. Sci.*, 2024, **15**(16), 6088–6094.

© 2025 The Author(s). Published by the Royal Society of Chemistry